

DESY-10-129

August 2010

Measurement of high- Q^2 charged current deep inelastic scattering cross sections with a longitudinally polarised positron beam at HERA

ZEUS Collaboration

Abstract

Measurements of the cross sections for charged current deep inelastic scattering in e^+p collisions with a longitudinally polarised positron beam are presented. The measurements are based on a data sample with an integrated luminosity of 132 pb^{-1} collected with the ZEUS detector at HERA at a centre-of-mass energy of 318 GeV. The total cross section is presented at positive and negative values of the longitudinal polarisation of the positron beams. The single-differential cross-sections $d\sigma/dQ^2$, $d\sigma/dx$ and $d\sigma/dy$ are presented for $Q^2 > 200 \text{ GeV}^2$. The reduced cross-section $\tilde{\sigma}$ is presented in the kinematic range $200 < Q^2 < 60\,000 \text{ GeV}^2$ and $0.006 < x < 0.562$. The measurements agree well with the predictions of the Standard Model. The results are used to determine a lower limit on the mass of a hypothetical right-handed W boson.

The ZEUS Collaboration

H. Abramowicz^{44,ag}, I. Abt³⁴, L. Adamczyk¹³, M. Adamus⁵³, R. Aggarwal⁷, S. Antonelli⁴, P. Antonioli³, A. Antonov³², M. Arneodo⁴⁹, V. Aushev^{26,ab}, Y. Aushev^{26,ab}, O. Bachynska¹⁵, A. Bamberger¹⁹, A.N. Barakbaev²⁵, G. Barbagli¹⁷, G. Bari³, F. Barreiro²⁹, D. Bartsch⁵, M. Basile⁴, O. Behnke¹⁵, J. Behr¹⁵, U. Behrens¹⁵, L. Bellagamba³, A. Bertolin³⁸, S. Bhadra⁵⁶, M. Bindi⁴, C. Blohm¹⁵, V. Bokhonov²⁶, T. Bołd¹³, E.G. Boos²⁵, K. Borras¹⁵, D. Boscherini³, D. Bot¹⁵, S.K. Boutle⁵¹, I. Brock⁵, E. Brownson⁵⁵, R. Brugnera³⁹, N. Brümmer³⁶, A. Bruni³, G. Bruni³, B. Brzozowska⁵², P.J. Bussey²⁰, J.M. Butterworth⁵¹, B. Bylsma³⁶, A. Caldwell³⁴, M. Capua⁸, R. Carlin³⁹, C.D. Catterall⁵⁶, S. Chekanov¹, J. Chwastowski^{12,f}, J. Ciborowski^{52,ak}, R. Ciesielski^{15,h}, L. Cifarelli⁴, F. Cindolo³, A. Contin⁴, A.M. Cooper-Sarkar³⁷, N. Coppola^{15,i}, M. Corradi³, F. Corriveau³⁰, M. Costa⁴⁸, G. D'Agostini⁴², F. Dal Corso³⁸, J. del Peso²⁹, R.K. Dementiev³³, S. De Pasquale^{4,b}, M. Derrick¹, R.C.E. Devenish³⁷, D. Dobur^{19,u}, B.A. Dolgoshein³², G. Dolinska²⁶, A.T. Doyle²⁰, V. Drugakov¹⁶, L.S. Durkin³⁶, S. Dusini³⁸, Y. Eisenberg⁵⁴, P.F. Ermolov^{33,†}, A. Eskreys¹², S. Fang^{15,j}, S. Fazio⁸, J. Ferrando³⁷, M.I. Ferrero⁴⁸, J. Figiel¹², M. Forrest²⁰, B. Foster³⁷, S. Fourletov^{50,w}, G. Gach¹³, A. Galas¹², E. Gallo¹⁷, A. Garfagnini³⁹, A. Geiser¹⁵, I. Gialas^{21,x}, L.K. Gladilin³³, D. Gladkov³², C. Glasman²⁹, O. Gogota²⁶, Yu.A. Golubkov³³, P. Göttlicher^{15,k}, I. Grabowska-Bold¹³, J. Grebenyuk¹⁵, I. Gregor¹⁵, G. Grigorescu³⁵, G. Grzelak⁵², C. Gwenlan^{37,ad}, T. Haas¹⁵, W. Hain¹⁵, R. Hamatsu⁴⁷, J.C. Hart⁴³, H. Hartmann⁵, G. Hartner⁵⁶, E. Hilger⁵, D. Hochman⁵⁴, R. Hori⁴⁶, K. Horton^{37,ae}, A. Hüttmann¹⁵, G. Iacobucci³, Z.A. Ibrahim¹⁰, Y. Iga⁴¹, R. Ingbir⁴⁴, M. Ishitsuka⁴⁵, H.-P. Jakob⁵, F. Januschek¹⁵, M. Jimenez²⁹, T.W. Jones⁵¹, M. Jüngst⁵, I. Kadenko²⁶, B. Kahle¹⁵, B. Kamaluddin^{10,†}, S. Kananov⁴⁴, T. Kanno⁴⁵, U. Karshon⁵⁴, F. Karstens^{19,v}, I.I. Katkov^{15,l}, M. Kaur⁷, P. Kaur^{7,d}, A. Keramidis³⁵, L.A. Khein³³, J.Y. Kim⁹, D. Kisielewska¹³, S. Kitamura^{47,ah}, R. Klanner²², U. Klein^{15,m}, E. Koffeman³⁵, P. Kooijman³⁵, Ie. Korol²⁶, I.A. Korzhavina³³, A. Kotański^{14,g}, U. Kötz¹⁵, H. Kowalski¹⁵, P. Kulinski⁵², O. Kuprash^{26,ac}, M. Kuze⁴⁵, A. Lee³⁶, B.B. Levchenko³³, A. Levy⁴⁴, V. Libov¹⁵, S. Limentani³⁹, T.Y. Ling³⁶, M. Lisovyi¹⁵, E. Lobodzinska¹⁵, W. Lohmann¹⁶, B. Lühr¹⁵, E. Lohrmann²², J.H. Loizides⁵¹, K.R. Long²³, A. Longhin³⁸, D. Lontkovskiy^{26,ac}, O.Yu. Lukina³³, P. Łuźniak^{52,al}, J. Maeda⁴⁵, S. Magill¹, I. Makarenko^{26,ac}, J. Malka^{52,al}, R. Mankel^{15,n}, A. Margotti³, G. Marini⁴², J.F. Martin⁵⁰, A. Mastroberardino⁸, T. Matsumoto^{24,y}, M.C.K. Mattingly², I.-A. Melzer-Pellmann¹⁵, S. Miglioranza^{15,o}, F. Mohamad Idris¹⁰, V. Monaco⁴⁸, A. Montanari¹⁵, J.D. Morris^{6,c}, B. Musgrave¹, K. Nagano²⁴, T. Namsoo^{15,p}, R. Nania³, D. Nicholass^{1,a}, A. Nigro⁴², Y. Ning¹¹, U. Noor⁵⁶, D. Notz¹⁵, R.J. Nowak⁵², A.E. Nuncio-Quiroz⁵, B.Y. Oh⁴⁰, N. Okazaki⁴⁶, K. Oliver³⁷, K. Olkiewicz¹², Yu. Onishchuk²⁶, O. Ota^{47,ai}, K. Papageorgiu²¹, A. Parenti¹⁵, E. Paul⁵, J.M. Pawlak⁵², B. Pawlik¹², P. G. Pelfer¹⁸, A. Pellegrino³⁵, W. Perlanski^{52,al}, H. Perrey²², K. Piotrkowski²⁸, P. Plucinski^{53,am}, N.S. Pokrovskiy²⁵, A. Polini³, A.S. Proskuryakov³³, M. Przybycień¹³, A. Raval¹⁵, D.D. Reeder⁵⁵, B. Reisert³⁴, Z. Ren¹¹, J. Repond¹, Y.D. Ri^{47,aj}, A. Robertson³⁷, P. Roloff¹⁵, E. Ron²⁹, I. Rubinsky¹⁵, M. Ruspa⁴⁹, R. Sacchi⁴⁸, A. Saliı̄²⁶, U. Samson⁵, G. Sartorelli⁴, A.A. Savin⁵⁵, D.H. Saxon²⁰, M. Schioppa⁸, S. Schlenstedt¹⁶, P. Schleper²², W.B. Schmidke³⁴, U. Schneekloth¹⁵, V. Schönberg⁵, T. Schörner-Sadenius¹⁵, J. Schwartz³⁰,

F. Sciulli¹¹, L.M. Shcheglova³³, R. Shehzadi⁵, S. Shimizu^{46,o}, I. Singh^{7,d}, I.O. Skillicorn²⁰, W. Słomiński¹⁴, W.H. Smith⁵⁵, V. Sola⁴⁸, A. Solano⁴⁸, D. Son²⁷, V. Sosnovtsev³², A. Spiridonov^{15,q}, H. Stadie²², L. Stanco³⁸, A. Stern⁴⁴, T.P. Stewart⁵⁰, A. Stifutkin³², P. Stopa¹², S. Suchkov³², G. Susinno⁸, L. Suszycki¹³, J. Sztuk-Dambietz²², D. Szuba^{15,r}, J. Szuba^{15,s}, A.D. Tapper²³, E. Tassi^{8,e}, J. Terrón²⁹, T. Theedt¹⁵, H. Tiecke³⁵, K. Tokushuku^{24,z}, O. Tomalak²⁶, J. Tomaszewska^{15,t}, T. Tsurugai³¹, M. Turcato²², T. Tymieniecka^{53,an}, C. Uribe-Estrada²⁹, M. Vázquez^{35,o}, A. Verbytskyi¹⁵, O. Viazlo²⁶, N.N. Vlasov^{19,w}, O. Volynets²⁶, R. Walczak³⁷, W.A.T. Wan Abdullah¹⁰, J.J. Whitmore^{40,af}, J. Whyte⁵⁶, L. Wiggers³⁵, M. Wing⁵¹, M. Wlasenko⁵, G. Wolf¹⁵, H. Wolfe⁵⁵, K. Wrona¹⁵, A.G. Yagües-Molina¹⁵, S. Yamada²⁴, Y. Yamazaki^{24,aa}, R. Yoshida¹, C. Youngman¹⁵, A.F. Żarnecki⁵², L. Zawiejski¹², O. Zenaiev²⁶, W. Zeuner^{15,o}, B.O. Zhautykov²⁵, N. Zhmak^{26,ab}, C. Zhou³⁰, A. Zichichi⁴, M. Zolko²⁶, D.S. Zotkin³³, Z. Zulkapli¹⁰

- 1 *Argonne National Laboratory, Argonne, Illinois 60439-4815, USA*^A
2 *Andrews University, Berrien Springs, Michigan 49104-0380, USA*
3 *INFN Bologna, Bologna, Italy*^B
4 *University and INFN Bologna, Bologna, Italy*^B
5 *Physikalisches Institut der Universität Bonn, Bonn, Germany*^C
6 *H.H. Wills Physics Laboratory, University of Bristol, Bristol, United Kingdom*^D
7 *Panjab University, Department of Physics, Chandigarh, India*
8 *Calabria University, Physics Department and INFN, Cosenza, Italy*^B
9 *Institute for Universe and Elementary Particles, Chonnam National University,*
10 *Kwangju, South Korea*
11 *Jabatan Fizik, Universiti Malaya, 50603 Kuala Lumpur, Malaysia*^E
12 *Nevis Laboratories, Columbia University, Irvington on Hudson, New York 10027,*
13 *USA*^F
14 *The Henryk Niewodniczanski Institute of Nuclear Physics, Polish Academy of*
15 *Sciences, Cracow, Poland*^G
16 *Faculty of Physics and Applied Computer Science, AGH-University of Science and*
17 *Technology, Cracow, Poland*^H
18 *Department of Physics, Jagellonian University, Cracow, Poland*
19 *Deutsches Elektronen-Synchrotron DESY, Hamburg, Germany*
20 *Deutsches Elektronen-Synchrotron DESY, Zeuthen, Germany*
21 *INFN Florence, Florence, Italy*^B
22 *University and INFN Florence, Florence, Italy*^B
23 *Fakultät für Physik der Universität Freiburg i.Br., Freiburg i.Br., Germany*
24 *School of Physics and Astronomy, University of Glasgow, Glasgow, United King-*
25 *dom*^D
26 *Department of Engineering in Management and Finance, Univ. of the Aegean,*
27 *Chios, Greece*
28 *Hamburg University, Institute of Experimental Physics, Hamburg, Germany*^I
29 *Imperial College London, High Energy Nuclear Physics Group, London, United*
30 *Kingdom*^D
31 *Institute of Particle and Nuclear Studies, KEK, Tsukuba, Japan*^J
32 *Institute of Physics and Technology of Ministry of Education and Science of Kaza-*
khstan, Almaty, Kazakhstan
33 *Institute for Nuclear Research, National Academy of Sciences, and Kiev National*
34 *University, Kiev, Ukraine*
35 *Kyungpook National University, Center for High Energy Physics, Daegu, South Ko-*
36 *rea*^K
37 *Institut de Physique Nucléaire, Université Catholique de Louvain, Louvain-la-Neuve,*
38 *Belgium*^L
39 *Departamento de Física Teórica, Universidad Autónoma de Madrid, Madrid,*
40 *Spain*^M
41 *Department of Physics, McGill University, Montréal, Québec, Canada H3A 2T8*^N
42 *Meiji Gakuin University, Faculty of General Education, Yokohama, Japan*^J
43 *Moscow Engineering Physics Institute, Moscow, Russia*^O

- 33 *Moscow State University, Institute of Nuclear Physics, Moscow, Russia*^P
34 *Max-Planck-Institut für Physik, München, Germany*
35 *NIKHEF and University of Amsterdam, Amsterdam, Netherlands*^Q
36 *Physics Department, Ohio State University, Columbus, Ohio 43210, USA*^A
37 *Department of Physics, University of Oxford, Oxford, United Kingdom*^D
38 *INFN Padova, Padova, Italy*^B
39 *Dipartimento di Fisica dell' Università and INFN, Padova, Italy*^B
40 *Department of Physics, Pennsylvania State University, University Park,
Pennsylvania 16802, USA*^F
41 *Polytechnic University, Sagamihara, Japan*^J
42 *Dipartimento di Fisica, Università 'La Sapienza' and INFN, Rome, Italy*^B
43 *Rutherford Appleton Laboratory, Chilton, Didcot, Oxon, United Kingdom*^D
44 *Raymond and Beverly Sackler Faculty of Exact Sciences, School of Physics,
Tel Aviv University, Tel Aviv, Israel*^R
45 *Department of Physics, Tokyo Institute of Technology, Tokyo, Japan*^J
46 *Department of Physics, University of Tokyo, Tokyo, Japan*^J
47 *Tokyo Metropolitan University, Department of Physics, Tokyo, Japan*^J
48 *Università di Torino and INFN, Torino, Italy*^B
49 *Università del Piemonte Orientale, Novara, and INFN, Torino, Italy*^B
50 *Department of Physics, University of Toronto, Toronto, Ontario, Canada M5S
1A7*^N
51 *Physics and Astronomy Department, University College London, London, United
Kingdom*^D
52 *Warsaw University, Institute of Experimental Physics, Warsaw, Poland*
53 *Institute for Nuclear Studies, Warsaw, Poland*
54 *Department of Particle Physics, Weizmann Institute, Rehovot, Israel*^S
55 *Department of Physics, University of Wisconsin, Madison, Wisconsin 53706, USA*^A
56 *Department of Physics, York University, Ontario, Canada M3J 1P3*^N

- A* supported by the US Department of Energy
- B* supported by the Italian National Institute for Nuclear Physics (INFN)
- C* supported by the German Federal Ministry for Education and Research (BMBF),
under contract No. 05 H09PDF
- D* supported by the Science and Technology Facilities Council, UK
- E* supported by an FRGS grant from the Malaysian government
- F* supported by the US National Science Foundation. Any opinion, findings and conclusions or recommendations expressed in this material are those of the authors and do not necessarily reflect the views of the National Science Foundation.
- G* supported by the Polish Ministry of Science and Higher Education as a scientific project No. DPN/N188/DESY/2009
- H* supported by the Polish Ministry of Science and Higher Education as a scientific project (2009-2010)
- I* supported by the German Federal Ministry for Education and Research (BMBF), under contract No. 05h09GUF, and the SFB 676 of the Deutsche Forschungsgemeinschaft (DFG)
- J* supported by the Japanese Ministry of Education, Culture, Sports, Science and Technology (MEXT) and its grants for Scientific Research
- K* supported by the Korean Ministry of Education and Korea Science and Engineering Foundation
- L* supported by FNRS and its associated funds (IISN and FRIA) and by an Inter-University Attraction Poles Programme subsidised by the Belgian Federal Science Policy Office
- M* supported by the Spanish Ministry of Education and Science through funds provided by CICYT
- N* supported by the Natural Sciences and Engineering Research Council of Canada (NSERC)
- O* partially supported by the German Federal Ministry for Education and Research (BMBF)
- P* supported by RF Presidential grant N 41-42.2010.2 for the Leading Scientific Schools and by the Russian Ministry of Education and Science through its grant for Scientific Research on High Energy Physics
- Q* supported by the Netherlands Foundation for Research on Matter (FOM)
- R* supported by the Israel Science Foundation
- S* supported in part by the MINERVA Gesellschaft für Forschung GmbH, the Israel Science Foundation (grant No. 293/02-11.2) and the US-Israel Binational Science Foundation

- a* also affiliated with University College London, United Kingdom
- b* now at University of Salerno, Italy
- c* now at Queen Mary University of London, United Kingdom
- d* also working at Max Planck Institute, Munich, Germany
- e* also Senior Alexander von Humboldt Research Fellow at Hamburg University, Institute of Experimental Physics, Hamburg, Germany
- f* also at Cracow University of Technology, Faculty of Physics, Mathematics and Applied Computer Science, Poland
- g* supported by the research grant No. 1 P03B 04529 (2005-2008)
- h* now at Rockefeller University, New York, NY 10065, USA
- i* now at DESY group FS-CFEL-1
- j* now at Institute of High Energy Physics, Beijing, China
- k* now at DESY group FEB, Hamburg, Germany
- l* also at Moscow State University, Russia
- m* now at University of Liverpool, United Kingdom
- n* on leave of absence at CERN, Geneva, Switzerland
- o* now at CERN, Geneva, Switzerland
- p* now at Goldman Sachs, London, UK
- q* also at Institute of Theoretical and Experimental Physics, Moscow, Russia
- r* also at INP, Cracow, Poland
- s* also at FPACS, AGH-UST, Cracow, Poland
- t* partially supported by Warsaw University, Poland
- u* now at Istituto Nucleare di Fisica Nazionale (INFN), Pisa, Italy
- v* now at Haase Energie Technik AG, Neumünster, Germany
- w* now at Department of Physics, University of Bonn, Germany
- x* also affiliated with DESY, Germany
- y* now at Japan Synchrotron Radiation Research Institute (JASRI), Hyogo, Japan
- z* also at University of Tokyo, Japan
- † deceased
- aa* now at Kobe University, Japan
- ab* supported by DESY, Germany
- ac* supported by the Bogolyubov Institute for Theoretical Physics of the National Academy of Sciences, Ukraine
- ad* STFC Advanced Fellow
- ae* nee Korcsak-Gorzo
- af* This material was based on work supported by the National Science Foundation, while working at the Foundation.
- ag* also at Max Planck Institute, Munich, Germany, Alexander von Humboldt Research Award
- ah* now at Nihon Institute of Medical Science, Japan
- ai* now at SunMelx Co. Ltd., Tokyo, Japan
- aj* now at Osaka University, Osaka, Japan

- ak* also at Łódź University, Poland
- al* member of Łódź University, Poland
- am* now at Lund University, Lund, Sweden
- an* also at University of Podlasie, Siedlce, Poland

1 Introduction

Deep inelastic scattering (DIS) of leptons off nucleons has proved to be a key process in the understanding of the structure of the proton and the Standard Model (SM). Neutral current (NC) DIS is mediated by the exchange of photons and Z bosons and is sensitive to all quark flavours. In contrast, at leading order, only down-type quarks and up-type antiquarks contribute to e^+p charged current (CC) DIS. Thus this process is a powerful probe of flavour-specific parton distribution functions (PDFs). The SM predicts that the cross section for charged current ep DIS depends linearly on the longitudinal polarisation of the incoming lepton beam. The cross section becomes zero for right-handed (left-handed) electron (positron) beams, due to the chiral nature of the weak interaction.

Using data taken at the HERA ep collider in the years 1994–2000 and 2004–2006, the H1 and ZEUS collaborations have reported measurements of the cross sections for CC DIS [1–15]. These measurements extend the kinematic region covered by fixed-target proton-structure measurements [16–19] to higher values of negative four-momentum-transfer squared, Q^2 .

This paper presents measurements of the cross sections for e^+p CC DIS with a longitudinally polarised positron beam. The measured cross sections are compared with the SM predictions and previous ZEUS measurements of e^+p CC DIS with an unpolarised positron beam [13]. Similar results in e^-p CC DIS have been published by the ZEUS Collaboration [15]. The total e^+p cross section in bins of polarisation is fitted and extrapolated to find the cross section for a fully left-handed polarised positron beam. The upper limit on this cross section is used to extract a lower limit on the mass of a hypothetical W boson which couples to right-handed particles.

This analysis is based on a data set with a five-fold increase in integrated luminosity compared to the previously published analysis of polarised e^+p CC DIS [14] and twice the integrated luminosity compared to the previously most precise published analysis of e^+p CC DIS (with unpolarised positrons) [13].

2 Kinematic variables and cross sections

Inclusive deep inelastic lepton-proton scattering can be described in terms of the kinematic variables x , y and Q^2 . The variable Q^2 is defined as $Q^2 = -q^2 = -(k - k')^2$ where k and k' are the four-momenta of the incoming and scattered lepton, respectively. Bjorken x is defined as $x = Q^2/2P \cdot q$ where P is the four-momentum of the incoming proton. The variable y is defined as $y = P \cdot q/P \cdot k$. The variables x , y and Q^2 are related by $Q^2 = sxy$, where $s = 4E_e E_p$ is the square of the lepton-proton centre-of-mass energy (neglecting the

masses of the incoming particles) and E_e and E_p are the energies of the incoming positron and proton, respectively.

The electroweak Born-level cross section for the CC reaction, $e^+p \rightarrow \bar{\nu}_e X$, with a longitudinally polarised positron beam can be expressed as [20]

$$\frac{d^2\sigma^{\text{CC}}}{dx dQ^2} = (1 + P_e) \frac{G_F^2}{4\pi x} \left(\frac{M_W^2}{M_W^2 + Q^2} \right)^2 \left[Y_+ F_2^{\text{CC}}(x, Q^2) - Y_- x F_3^{\text{CC}}(x, Q^2) - y^2 F_L^{\text{CC}}(x, Q^2) \right],$$

where G_F is the Fermi constant, M_W is the mass of the W boson and $Y_{\pm} = 1 \pm (1 - y)^2$. The longitudinal polarisation of the positron beam, P_e , is defined as

$$P_e = \frac{N_R - N_L}{N_R + N_L},$$

where N_R and N_L are the numbers of right- and left-handed positrons in the beam.

The longitudinal structure function, F_L^{CC} , is negligible except at values of y close to 1. At leading order in QCD, the structure functions F_2^{CC} and $x F_3^{\text{CC}}$ for e^+p collisions may be written in terms of sums and differences of quark and anti-quark PDFs as follows:

$$F_2^{\text{CC}} = x[d(x, Q^2) + s(x, Q^2) + \bar{u}(x, Q^2) + \bar{c}(x, Q^2)],$$

$$x F_3^{\text{CC}} = x[d(x, Q^2) + s(x, Q^2) - \bar{u}(x, Q^2) - \bar{c}(x, Q^2)],$$

where, for example, the PDF $d(x, Q^2)$ gives the number density of down quarks with momentum-fraction x at a given Q^2 . Since the top-quark mass is large and the off-diagonal elements of the CKM matrix are small [21], the contribution from third-generation quarks may be ignored [22].

The reduced cross section, $\tilde{\sigma}$, is defined as

$$\tilde{\sigma} = \left[\frac{G_F^2}{2\pi x} \left(\frac{M_W^2}{M_W^2 + Q^2} \right)^2 \right]^{-1} \frac{d^2\sigma^{\text{CC}}}{dx dQ^2}.$$

At leading order in QCD, the unpolarised reduced cross section depends on the quark momentum distributions as follows:

$$\tilde{\sigma}(e^+p \rightarrow \bar{\nu}_e X) = x [(\bar{u} + \bar{c} + (1 - y)^2(d + s))].$$

3 Experimental apparatus

A detailed description of the ZEUS detector can be found elsewhere [23]. A brief outline of the components most relevant for this analysis is given below.

In the kinematic range of the analysis, charged particles were tracked in the central tracking detector (CTD) [24], the microvertex detector (MVD) [25] and the straw tube tracker (STT) [26]. The CTD and the MVD operated in a magnetic field of 1.43 T provided by a thin superconducting solenoid. The CTD consisted of 72 cylindrical drift chamber layers, organised in nine superlayers covering the polar-angle¹ region $15^\circ < \theta < 164^\circ$. The MVD silicon tracker consisted of a barrel (BMVD) and a forward (FMVD) section. The BMVD provided polar-angle coverage for tracks with three measurements from 30° to 150° . The FMVD extended the polar-angle coverage in the forward region down to 7° . The STT consisted of 48 sectors of two different sizes. Each sector contained 192 (small sector) or 264 (large sector) straws of diameter 7.5 mm arranged into 3 layers. The sectors were trapezoidal in shape and each subtended an azimuthal angle of 60° ; six sectors formed a superlayer. A particle passing through the complete STT traversed 8 superlayers, which were rotated around the beam direction at angles of 30° or 15° to each other. The STT covered the polar-angle region $5^\circ < \theta < 23^\circ$.

The high-resolution uranium–scintillator calorimeter (CAL) [27] consisted of three parts: the forward (FCAL), the barrel (BCAL) and the rear (RCAL) calorimeter, covering 99.7% of the solid angle around the nominal interaction point. Each part was subdivided transversely into towers and longitudinally into one electromagnetic section (EMC) and either one (in RCAL) or two (in BCAL and FCAL) hadronic sections (HAC). The smallest subdivision of the calorimeter was called a cell. The CAL relative energy resolutions, as measured under test-beam conditions, were $\sigma(E)/E = 0.18/\sqrt{E}$ for positrons and $\sigma(E)/E = 0.35/\sqrt{E}$ for hadrons, with E in GeV. The timing resolution of the CAL was better than 1 ns for energy deposits exceeding 4.5 GeV.

An iron structure that surrounded the CAL was instrumented as a backing calorimeter (BAC) [28] to measure energy leakage from the CAL. Muon chambers in the forward [23], barrel and rear regions [29] were used in this analysis to veto background events induced by cosmic-ray or beam-halo muons.

The luminosity was measured using the Bethe-Heitler reaction $ep \rightarrow e\gamma p$ with the luminosity detector which consisted of two independent systems, a photon calorimeter [30–32] and a magnetic spectrometer [33].

The lepton beam in HERA became naturally transversely polarised through the Sokolov-Ternov effect [34, 35]. The characteristic build-up time for the HERA accelerator was approximately 40 minutes. Spin rotators on either side of the ZEUS detector changed the transverse polarisation of the beam into longitudinal polarisation and back again.

¹ The ZEUS coordinate system is a right-handed Cartesian system, with the Z axis pointing in the proton beam direction, referred to as the “forward direction”, and the X axis pointing towards the centre of HERA. The coordinate origin is at the nominal interaction point.

The positron beam polarisation was measured using two independent polarimeters, the transverse polarimeter (TPOL) [36] and the longitudinal polarimeter (LPOL) [37]. Both devices exploited the spin-dependent cross section for Compton scattering of circularly polarised photons off positrons to measure the beam polarisation. The luminosity and polarisation measurements were made over time intervals that were much shorter than the polarisation build-up time.

The measurements are based on data samples collected with the ZEUS detector in 2006 and 2007 when HERA collided protons of energy 920 GeV with positrons of energy 27.5 GeV, yielding collisions at a centre-of-mass energy of 318 GeV. The integrated luminosities of the data sample were 75.8 pb^{-1} and 56.0 pb^{-1} at mean luminosity-weighted polarisations of $+0.33$ and -0.36 , respectively. Runs with mean absolute polarisation less than 15% were rejected so that the polarisation measurement was reliable with a well understood systematic uncertainty. Figure 1 shows the luminosity collected as a function of the longitudinal polarisation of the positron beam.

4 Monte Carlo simulation

Monte Carlo (MC) simulation was used to determine the efficiency for selecting events, the accuracy of kinematic reconstruction, to estimate the background rate and to extract cross sections for the full kinematic region from the data. A sufficient number of events was generated to ensure that uncertainties from MC statistics were negligible. The MC samples were normalised to the total integrated luminosity of the data.

Charged current DIS events, including electroweak radiative effects, were simulated using the HERACLES 4.6.6 [38] program with the DJANGO 1.6 [39] interface to the MC generators that provide the hadronisation. Initial-state radiation, vertex and propagator corrections and two-boson exchange are included in HERACLES. The parameters of the SM were set to the PDG [21] values. The events were generated using the CTEQ5D [40] PDFs. The colour-dipole model of ARIADNE 4.12 [41] was used to simulate $\mathcal{O}(\alpha_S)$ plus leading-logarithmic corrections to the result of the quark-parton model. ARIADNE uses the Lund string model of JETSET 7.4.1 [42] for the hadronisation. A set of NC DIS events generated with DJANGO was used to estimate the NC contamination in the CC sample. Photoproduction background was estimated using events simulated with HERWIG 5.9 [43]. Events simulated with GRAPE 1.1 [44] and EPVEC 1.0 [45] were used to estimate the background contribution from di-lepton and single- W production, respectively.

The ZEUS detector response was simulated using a program based on GEANT 3.21 [46]. The generated events were passed through the detector simulation, subjected to the same trigger requirements as the data and processed by the same reconstruction programs.

5 Reconstruction of kinematic variables

The main experimental signature of CC DIS events at HERA is large missing transverse momentum, $\vec{P}_{T,\text{miss}}$. Figure 2 shows such an event as observed using the ZEUS detector. The struck quark gives rise to one or more jets of hadrons and the energetic final-state neutrino escapes detection, leaving a large imbalance in the transverse momentum observed in the detector. The vector $\vec{P}_{T,\text{miss}}$ is derived from the total visible hadronic momentum vector, \vec{P}_T , by $\vec{P}_{T,\text{miss}} = -\vec{P}_T$, where

$$\vec{P}_T = (P_x, P_y) = \left(\sum_i E_i \sin \theta_i \cos \phi_i, \sum_i E_i \sin \theta_i \sin \phi_i \right).$$

The sums run over all CAL energy deposits, E_i , and θ_i and ϕ_i are the polar and azimuthal angles of the calorimeter deposit i as viewed from the interaction vertex [15]. The polar angle of the hadronic system, γ_h , is defined as

$$\cos \gamma_h = \frac{\left(\vec{P}_T\right)^2 - \delta^2}{\left(\vec{P}_T\right)^2 + \delta^2},$$

where $\delta = \sum_i E_i(1 - \cos \theta_i) = \sum_i (E - P_Z)_i$. In the naive quark-parton model, γ_h is the angle of the scattered quark. Finally, the total transverse energy, E_T , is given by $E_T = \sum_i E_i \sin \theta_i$.

The ratio of the parallel, V_P , and antiparallel, V_{AP} , components of the hadronic transverse momentum can be used to distinguish CC DIS from photoproduction events. These variables are defined as

$$V_P = \sum_i \vec{P}_{T,i} \cdot \vec{n} \quad \text{for } \vec{P}_{T,i} \cdot \vec{n} > 0,$$

$$V_{AP} = - \sum_i \vec{P}_{T,i} \cdot \vec{n} \quad \text{for } \vec{P}_{T,i} \cdot \vec{n} < 0,$$

where the sums are performed over all calorimeter deposits and $\vec{n} = \vec{P}_T/P_T$.

The kinematic variables were reconstructed using the Jacquet-Blondel method [47]: $y_{\text{JB}} = \delta/(2E_e)$, $Q_{\text{JB}}^2 = P_{T,\text{miss}}^2/(1 - y_{\text{JB}})$, and $x_{\text{JB}} = Q_{\text{JB}}^2/(sy_{\text{JB}})$. The resolution in Q^2 is $\approx 24\%$. The resolution in x improves from $\approx 26\%$ at $x = 0.0078$ to $\approx 9\%$ at $x = 0.65$. The resolution in y ranges from $\approx 15\%$ at $y = 0.05$ to $\approx 8\%$ at $y = 0.83$.

6 Charged current event selection

Charged current DIS candidate events were selected by requiring a large $P_{T,\text{miss}}$ in the event. Backgrounds to CC DIS arise from high- E_T events in which the finite energy resolution of the CAL or energy that escapes detection can lead to significant missing transverse momentum. Non- ep events such as beam-gas interactions, beam-halo muons or cosmic rays can also cause substantial imbalance in the measured transverse momentum and constitute additional sources of background. The following criteria were imposed to select CC DIS events and reject these backgrounds.

6.1 Trigger selection

Events were selected using the ZEUS three-level trigger system [23, 48, 49]. At the first level, coarse calorimeter and tracking information was available. Events were selected using criteria based on the energy, transverse energy and missing transverse momentum measured in the calorimeter. Generally, events were triggered with low thresholds on these quantities if a coincidence with CTD tracks from the event vertex occurred, while higher thresholds were required for events with no CTD tracks.

At the second level, timing information from the calorimeter was used to reject events inconsistent with the bunch-crossing time. In addition, the topology of the CAL energy deposits was used to reject background events. In particular, a tighter cut was made on missing transverse momentum, since the resolution in this variable was better at the second than at the first level.

At the third level, full track reconstruction and vertex finding were performed and used to reject candidate events with a vertex inconsistent with an ep interaction. Cuts were applied to calorimeter quantities and reconstructed tracks to reduce beam-gas contamination further.

6.2 Offline selection

For all events, the kinematic variables were recalculated using the Z -coordinate of the event vertex (Z_{vtx}) determined from charged-particle tracks. The requirements for event selection are given below:

- kinematic cuts: events were required to satisfy $Q_{\text{JB}}^2 > 200 \text{ GeV}^2$ and $y_{\text{JB}} < 0.9$. These requirements restricted the event sample to a region where the resolution of the kinematic quantities is good and the background is small;

- missing transverse momentum: $P_{T,\text{miss}} > 12 \text{ GeV}$ was required and, in addition, the missing transverse momentum excluding the calorimeter cells adjacent to the forward beam hole, $P'_{T,\text{miss}}$, was required to exceed 10 GeV ;
- primary interaction vertex: events were required to satisfy $|Z_{\text{vtx}}| < 30 \text{ cm}$. The improved tracking information compared to the previous charged current analysis [15] allowed the requirement of a reconstructed primary vertex in the full phase-space. This requirement strongly suppressed non- ep backgrounds;
- rejection of photoproduction and di-leptons: for events with $P_{T,\text{miss}} < 20 \text{ GeV}$, $V_{AP}/V_P < 0.25$ was required; for all other events, $V_{AP}/V_P < 0.35$ was required. These requirements demanded an azimuthally collimated energy flow. In addition, for all events, the azimuthal-angle difference, $\Delta\phi$, between the missing transverse momentum measured by the tracks and that measured by the calorimeter was required to be less than 90° for all events;
- rejection of NC DIS: NC DIS events with a poorly measured scattered positron or hadronic jet can have significant missing transverse momentum. Events with $\delta > 30 \text{ GeV}$ and an isolated electromagnetic cluster in the calorimeter [50, 51] were rejected as detailed in a previous publication [15];
- rejection of remaining non- ep background: interactions between the beams and residual gas in the beam pipe or upstream accelerator components can lead to events with significant missing transverse momentum. However, for these interactions, the arrival times of energy deposits in the calorimeter are inconsistent with the bunch-crossing time and were used to reject such events. Events caused by interactions with the residual gas are characterised by a large fraction of tracks not associated with the ep interaction vertex; such events were rejected by applying a cut in two dimensions on the number of vertex tracks, N_{VtxTrks} , versus the total number of tracks, N_{Trks} . This cut was $N_{\text{VtxTrks}} > 0.125 \cdot (N_{\text{Trks}} - 20)$. Vertex tracks were required to originate in the MVD or in the first superlayer of the CTD and to have a polar angle in the range of $15^\circ < \theta < 160^\circ$. Requirements on energy fractions in the calorimeter cells plus muon-finding algorithms based on tracking, calorimeter and muon chamber information were used to reject events caused by cosmic rays or muons in the beam halo.

A total of 2327 data events satisfied all criteria in the positive-polarisation sample and 821 events in the negative-polarisation sample. The background contamination was estimated to be typically less than 1.5%, but reached 8% in the lowest- Q^2 bin and 21% in the lowest- x bin of the negative-polarisation sample. Similarly, it was typically less than 1% but reached almost 4% in the lowest- Q^2 bin and 10% in the lowest- x bin of the positive-polarisation sample. For the combined sample (positive and negative polarisations) the estimated number of background events was 19, 11 and 6.6 for photoproduction, single- W

production and di-lepton events, respectively. The di-lepton background was dominated by $\mu\mu$ and $\tau\tau$ events. The contamination from NC events was estimated to be very small (0.7 events for the combined sample). Non- ep backgrounds were negligible. Figure 3 compares the distributions of data events entering the final CC sample with the MC expectation for the sum of the CC signal and ep background events. The MC simulations give a reasonable description of the data.

7 Cross-section determination

The measured cross section in a particular kinematic bin, for example in $d\sigma/dQ^2$, was determined from

$$\frac{d\sigma_{\text{Born}}}{dQ^2} = \frac{N_{\text{data}} - N_{\text{bg}}}{N_{\text{MC}}} \cdot \frac{d\sigma_{\text{Born}}^{\text{SM}}}{dQ^2},$$

where N_{data} is the number of data events, N_{bg} is the number of background events estimated from the MC simulation and N_{MC} is the number of signal MC events. The Standard Model prediction, $\frac{d\sigma_{\text{Born}}^{\text{SM}}}{dQ^2}$, is evaluated in the on-shell scheme using the PDG values for the electroweak parameters and the same PDF set (CTEQ5D) [40] used to generate the MC data. A similar procedure was used for $d\sigma/dx$, $d\sigma/dy$ and the reduced cross section. Consequently, the acceptance, as well as the bin-centring and radiative corrections were all taken from the MC simulation. The equation above includes the extrapolation of the single-differential cross-sections $d\sigma/dQ^2$ and $d\sigma/dx$ to the full y range.

8 Systematic uncertainties

Different systematic uncertainties in the measured cross sections were determined using one of two methods [52]. The first set of systematic uncertainties relies on MC simulations and was calculated by changing relevant parameters of the analysis by their estimated errors and repeating the extraction of the cross sections. The difference between the nominal cross section and that obtained from the modified analysis gave an estimate of the systematic uncertainty in each bin. The second method of calculating systematic uncertainties exploited the similarity between NC and CC hadronic final states. The following systematics were determined using the first method:

- calorimeter energy scale: the relative uncertainty of the hadronic energy scale was 2%. The variation of the energy scale for each of the calorimeters simultaneously up or down by this amount gave the systematic uncertainty on the total measured energy in

the calorimeter. The resulting uncertainties in the measured cross sections were $\approx 1\%$ for the total cross sections and for the single-differential cross sections were typically within $\pm 3\%$, but increased to $\pm(25 - 33)\%$ in the highest- Q^2 and highest- x bins. The uncertainties reached 35% in the highest- Q^2 and highest- x reduced cross-section bin;

- efficiency of the FLT tracking: the charged current MC was corrected for observed differences in the CTD tracking efficiency between data and MC at the first-level trigger [52]. The correction was derived from independent samples of NC data and NC MC events with the scattered electron removed in order to simulate CC events (pseudo-CC). The mean correction was $\approx 3.5\%$ for the positive-polarisation sample and $\approx 5\%$ for the negative-polarisation sample. The uncertainty on this correction was 50% of its value. The resulting uncertainties on the total cross sections were less than 1.5% and for the single-differential and reduced cross sections were typically 1 – 2% and were always less than 4%;
- background subtraction: the uncertainty in the small contribution from photoproduction was estimated. The V_{AP}/V_P distribution was plotted for data and MC events with all selection cuts applied except for the cut on V_{AP}/V_P . A χ^2 fit of the MC to the data distribution was performed, varying the normalisation of the photoproduction MC until it produced the best description of the data. The fit resulted in a normalisation factor of $0.880^{+0.090}_{-0.085}$. The nominal photoproduction sample was therefore scaled by a factor of 0.970 and by a factor of 0.795, resulting in very small modifications of less than 0.2% to the cross sections.

In the second method, a set of NC DIS data events with the scattered positron removed (pseudo-CC data) was reweighted to the Q^2 and x of the CC DIS MC. In order to estimate the bias introduced into the measurements from an imperfect description of the data by the MC simulation, the efficiencies for each of the selection criteria were measured using the hadronic final state in NC DIS data and compared to those obtained with the CC MC. The differences in the efficiencies between the two samples were taken as estimates of the systematic uncertainties which were typically within $\pm 3\%$.

The individual uncertainties were added in quadrature separately for the positive and negative deviations from the nominal cross section values to obtain the total systematic uncertainty.

The uncertainties on the electroweak corrections to CC DIS are less than 0.5% [53]. No uncertainty was included in the measured cross sections from this source.

The relative uncertainty in the measured polarisation was 3.6% using the LPOL and 4.2% using the TPOL. The choice of polarimeter measurement was made on a run-by-run basis depending on which was active the longer, in order to maximise the luminosity. For the final selection, the TPOL was used for 64% (24%) of the negative (positive)

polarisation run period. The combined, luminosity-weighted systematic uncertainty on the polarisation measurement was 4.0% (3.7%) for negative (positive) polarisation. The uncertainty of 2.6% on the measured total luminosity was not included in the differential cross-section figures or the tables.

9 Results

The total cross section, corrected to the Born level in the electroweak interaction, for e^+p CC DIS in the kinematic region $Q^2 > 200 \text{ GeV}^2$ was measured to be

$$\sigma^{\text{CC}}(P_e = -0.36) = 22.9 \pm 0.82(\text{stat.}) \pm 0.60(\text{lumi.}) \pm 0.40(\text{syst.}) \text{ pb},$$

$$\sigma^{\text{CC}}(P_e = +0.33) = 48.0 \pm 1.01(\text{stat.}) \pm 1.25(\text{lumi.}) \pm 0.77(\text{syst.}) \text{ pb}.$$

The total cross section is shown as a function of the longitudinal polarisation of the lepton beam in Fig. 4, including previous ZEUS measurements from both e^-p and e^+p data [12, 13, 15] and previous H1 measurements from e^+p data [8]. The H1 measurements were scaled to the kinematic region of this analysis. The uncertainty in the measured luminosity is included in the systematic uncertainty in Fig. 4. The data are compared to the SM predictions evaluated at next-to-leading order in QCD [54] using the HERAPDF1.0 [55], ZEUS-JETS [56], CTEQ6.6 [57] and MSTW2008 [58] PDFs, which describe the data well.

The single-differential cross-sections $d\sigma/dQ^2$, $d\sigma/dx$ and $d\sigma/dy$ for CC DIS are shown in Figs. 5, 6 and 7 for $Q^2 > 200 \text{ GeV}^2$ and given in Tables 1, 2 and 3, respectively. The cross sections are well described by the SM evaluated using the HERAPDF1.0, ZEUS-JETS, CTEQ6.6 and MSTW2008 PDFs. The precision of the data is comparable to the uncertainties in the SM predictions; therefore these data have the potential to constrain the PDFs further.

The reduced cross-section $\tilde{\sigma}$ was measured in the kinematic range $200 < Q^2 < 60\,000 \text{ GeV}^2$ and $0.006 < x < 0.562$ and is shown as a function of x at fixed values of Q^2 in Figs. 8 and 9 and given in Tables 4, 5 and 6. The data points are shown separately for positive and negative polarisation in Fig. 8 and are shown for the entire data set in Fig. 9, corrected to $P_e = 0$ using the SM prediction from HECTOR using CTEQ5D PDFs. The predictions of the SM evaluated using the HERAPDF1.0, ZEUS-JETS, CTEQ6.6 and MSTW2008 PDFs give a good description of the data. The contributions from the PDF combinations $(d+s)$ and $(\bar{u}+\bar{c})$, obtained in the $\overline{\text{MS}}$ scheme from the HERAPDF1.0 PDFs, are shown separately.

The SM W boson couples only to left-handed fermions and right-handed anti-fermions. Therefore, the angular distribution of the scattered quark in $e^+\bar{q}$ CC DIS will be flat in

the positron-quark centre-of-mass scattering angle, θ^* , while it will exhibit a $(1 + \cos \theta^*)^2$ distribution in e^+q scattering. Since $(1 - y)^2 \propto (1 + \cos \theta^*)^2$, the helicity structure of CC interactions can be illustrated by plotting the reduced cross section versus $(1 - y)^2$ in bins of x , see Section 2. The measurement is shown in Fig. 10 and is well described by the SM. At leading order in QCD, the intercept of the prediction gives the $(\bar{u} + \bar{c})$ contribution, while the slope gives the $(d + s)$ contribution.

The CC e^+p DIS cross section becomes zero for fully left-handed positron beams, thus a non-zero cross section at $P_e = -1$ might point to the existence of a right-handed W boson, W_R , and right-handed neutrinos, ν_R [59,60]. The program HECTOR was used to calculate the cross section for right-handed CC interactions in e^+p DIS as a function of the mass of the W_R , M_{W_R} . It was assumed that the coupling strength and propagator dependence on the mass of the boson are the same as in SM CC interactions. The outgoing right-handed neutrinos were assumed to be light. A linear function was fit to the total cross section in 8 bins of polarisation, including the previous ZEUS measurement of unpolarised e^+p CC DIS, and extrapolated to $P_e = -1$. The fit and extrapolation to $P_e = -1$ is shown in Fig. 11. The cross sections measured in each bin are given in Table 7. The upper limit on the cross section was converted to a lower limit on M_{W_R} :

$$\sigma^{\text{CC}}(P_e = -1) < 2.9 \text{ pb at } 95\% \text{ CL,}$$

$$M_{W_R} > 198 \text{ GeV at } 95\% \text{ CL.}$$

The limit on M_{W_R} set in this analysis is complementary to the limits obtained from direct searches [21,61–64]. In the direct searches, the W boson is time-like, whereas the limit from this analysis is for a space-like W .

10 Summary

The cross sections for charged current deep inelastic scattering in e^+p collisions with longitudinally polarised positron beams have been measured. The measurements are based on a data sample with an integrated luminosity of 132 pb^{-1} collected with the ZEUS detector at HERA at a centre-of-mass energy of 318 GeV . The total cross section is given for positive and negative values of the longitudinal polarisation of the positron beam. In addition, the single-differential cross-sections $d\sigma/dQ^2$, $d\sigma/dx$ and $d\sigma/dy$ for $Q^2 > 200 \text{ GeV}^2$ are measured. The reduced cross section is presented in the kinematic range $200 < Q^2 < 60\,000 \text{ GeV}^2$ and $0.006 < x < 0.562$. The measured cross sections are well described by the predictions of the Standard Model. Finally, a lower limit on the mass of a hypothetical right-handed W boson is extracted from the upper limit of the cross section at $P_e = -1$. The limit obtained is $M_{W_R} > 198 \text{ GeV}$ at 95% CL.

Acknowledgements

We appreciate the contributions to the construction and maintenance of the ZEUS detector of many people who are not listed as authors. The HERA machine group and the DESY computing staff are especially acknowledged for their success in providing excellent operation of the collider and the data-analysis environment. We thank the DESY directorate for their strong support and encouragement.

References

- [1] H1 Coll., T. Ahmed et al., Phys. Lett. **B 324**, 241 (1994).
- [2] H1 Coll., S. Aid et al., Z. Phys. **C 67**, 565 (1995).
- [3] H1 Coll., S. Aid et al., Phys. Lett. **B 379**, 319 (1996).
- [4] H1 Coll., C. Adloff et al., Eur. Phys. J. **C 13**, 609 (2000).
- [5] H1 Coll., C. Adloff et al., Eur. Phys. J. **C 19**, 269 (2001).
- [6] H1 Coll., C. Adloff et al., Eur. Phys. J. **C 21**, 33 (2001).
- [7] H1 Coll., C. Adloff et al., Eur. Phys. J. **C 30**, 1 (2003).
- [8] H1 Coll., A. Aktas et al., Phys. Lett. **B 634**, 173 (2005).
- [9] ZEUS Coll., M. Derrick et al., Phys. Rev. Lett. **75**, 1006 (1995).
- [10] ZEUS Coll., M. Derrick et al., Z. Phys. **C 72**, 47 (1996).
- [11] ZEUS Coll., J. Breitweg et al., Eur. Phys. J. **C 12**, 411 (2000). Erratum in Eur. Phys. J. **C 27**, 305 (2003).
- [12] ZEUS Coll., S. Chekanov et al., Phys. Lett. **B 539**, 197 (2002). Erratum in Phys. Lett. **B 552**, 308 (2003).
- [13] ZEUS Coll., S. Chekanov et al., Eur. Phys. J. **C 32**, 1 (2003).
- [14] ZEUS Coll., S. Chekanov et al., Phys. Lett. **B 637**, 28 (2006).
- [15] ZEUS Coll., S. Chekanov et al., Eur. Phys. J. **C 61**, 223 (2009).
- [16] CDHS Coll., H. Abramowicz et al., Z. Phys. **C 25**, 29 (1984).
- [17] CDHSW Coll., J.P. Berge et al., Z. Phys. **C 49**, 187 (1991).
- [18] CCFR Coll., E. Oltman et al., Z. Phys. **C 53**, 51 (1992).
- [19] BEBC Coll., G.T. Jones et al., Z. Phys. **C 62**, 575 (1994).
- [20] R. Devenish and A. Cooper-Sarkar, *Deep Inelastic Scattering*. Oxford University Press, 2003.
- [21] Particle Data Group, C. Amsler et al., Phys. Lett. **B667**, 1 (2008).
- [22] U.F. Katz, *Deep-Inelastic Positron-Proton Scattering in the High-Momentum-Transfer Regime of HERA*, Springer Tracts in Modern Physics, Vol. 168. Springer, Berlin, Heidelberg, 2000.
- [23] ZEUS Coll., U. Holm (ed.), *The ZEUS Detector*. Status Report (unpublished), DESY (1993), available on <http://www-zeus.desy.de/bluebook/bluebook.html>.

- [24] N. Harnew et al., Nucl. Inst. Meth. **A 279**, 290 (1989);
B. Foster et al., Nucl. Phys. Proc. Suppl. **B 32**, 181 (1993);
B. Foster et al., Nucl. Inst. Meth. **A 338**, 254 (1994).
- [25] A. Polini et al., Nucl. Inst. Meth. **A 581**, 656 (2007).
- [26] S. Fourletov, Nucl. Inst. Meth. **A 535**, 191 (2004).
- [27] M. Derrick et al., Nucl. Inst. Meth. **A 309**, 77 (1991);
A. Andresen et al., Nucl. Inst. Meth. **A 309**, 101 (1991);
A. Caldwell et al., Nucl. Inst. Meth. **A 321**, 356 (1992);
A. Bernstein et al., Nucl. Inst. Meth. **A 336**, 23 (1993).
- [28] H. Abramowicz et al., Nucl. Inst. Meth. **A 313**, 126 (1992).
- [29] G. Abbiendi et al., Nucl. Inst. Meth. **A 333**, 342 (1993).
- [30] J. Andruszków et al., Preprint DESY-92-066, DESY, 1992.
- [31] ZEUS Coll., M. Derrick et al., Z. Phys. **C 63**, 391 (1994).
- [32] J. Andruszków et al., Acta Phys. Pol. **B 32**, 2025 (2001).
- [33] M. Helbich et al., Nucl. Inst. Meth. **A 565**, 572 (2006).
- [34] A.A. Sokolov and I.M. Ternov, Sov. Phys. Dokl. **8**, 1203 (1964).
- [35] V.N. Baier and V.A. Khoze, Sov. J. Nucl. Phys. **B 9**, 238 (1969).
- [36] D.P. Barber et al., Nucl. Inst. Meth. **A 329**, 79 (1993).
- [37] M. Beckmann et al., Nucl. Inst. Meth. **A 479**, 334 (2002).
- [38] A. Kwiatkowski, H. Spiesberger and H.-J. Möhring, Comp. Phys. Comm. **69**, 155 (1992). Also in *Proc. Workshop Physics at HERA*, eds. W. Buchmüller and G. Ingelman, (DESY, Hamburg, 1991);
H. Spiesberger, *An Event Generator for ep Interactions at HERA Including Radiative Processes (Version 4.6)*, 1996, available on
<http://www.desy.de/~hspiesb/heracles.html>.
- [39] H. Spiesberger, *HERACLES and DJANGO: Event Generation for ep Interactions at HERA Including Radiative Processes*, 1998, available on
<http://www.desy.de/~hspiesb/djangoh.html>.
- [40] CTEQ Coll., H.L. Lai et al., Eur. Phys. J. **C 12**, 375 (2000).
- [41] L. Lönnblad, Comp. Phys. Comm. **71**, 15 (1992).
- [42] T. Sjöstrand, Comp. Phys. Comm. **39**, 347 (1986);
T. Sjöstrand and M. Bengtsson, Comp. Phys. Comm. **43**, 367 (1987);
T. Sjöstrand, Comp. Phys. Comm. **82**, 74 (1994).

- [43] G. Marchesini et al., *Comp. Phys. Comm.* **67**, 465 (1992).
- [44] T. Abe, *Comp. Phys. Comm.* **136**, 126 (2001).
- [45] U. Baur, J.A.M. Vermaseren and D. Zeppenfeld, *Nucl. Phys.* **B 375**, 3 (1992).
- [46] R. Brun et al., *GEANT3*, Technical Report CERN-DD/EE/84-1, CERN, 1987.
- [47] F. Jacquet and A. Blondel, *Proceedings of the Study for an ep Facility for Europe*, U. Amaldi (ed.), p. 391. Hamburg, Germany (1979). Also in preprint DESY 79/48.
- [48] W.H. Smith, K. Tokushuku and L.W. Wiggers, *Proc. Computing in High-Energy Physics (CHEP), Annecy, France, Sept. 1992*, C. Verkerk and W. Wojcik (eds.), p. 222. CERN, Geneva, Switzerland (1992). Also in preprint DESY 92-150B.
- [49] P.D. Allfrey et al., *Nucl. Inst. Meth.* **A 580**, 1257 (2007).
- [50] H. Abramowicz, A. Caldwell and R. Sinkus, *Nucl. Inst. Meth.* **A 365**, 508 (1995).
- [51] R. Sinkus and T. Voss, *Nucl. Inst. Meth.* **A 391**, 360 (1997).
- [52] K. Oliver. Ph.D. Thesis, University of Oxford, 2010. Unpublished.
- [53] V. Makarenko. Private communication.
- [54] J. Ferrando, *DISPred*. <http://projects.hepforge.org/dispred/>.
- [55] H1 and ZEUS Colls., F.D. Aaron et al., *JHEP* **01**, 109 (2010).
- [56] ZEUS Coll., S. Chekanov et al., *Eur. Phys. J.* **C 42**, 1 (2005).
- [57] CTEQ Coll., P.M. Nadolsky et al., *Phys. Rev.* **D 78**, 013004 (2008).
- [58] A.D. Martin et al., *Eur. Phys. J.* **C 63**, 189 (2009).
- [59] G. Senjanovic and R.N. Mohapatra, *Phys. Rev.* **D 12**, 1502 (1975).
- [60] R.N. Mohapatra and J.C. Pati, *Phys. Rev.* **D 11**, 2558 (1975).
- [61] UA2 Coll., J. Alitti et al., *Nucl. Phys.* **B 400**, 3 (1993).
- [62] DØ Coll., V.M. Abazov et al., *Phys. Rev. Lett.* **100**, 211803 (2008).
- [63] CDF Coll., T. Aaltonen et al., *Phys. Rev. Lett.* **103**, 041801 (2009).
- [64] DØ Coll., V.M. Abazov et al., *Phys. Rev. Lett.* **100**, 031804 (2008).

Q^2 range (GeV ²)	Q^2 (GeV ²)	$d\sigma/dQ^2$ (pb/ GeV ²)	
		$P_e = +0.33$	$P_e = -0.36$
200 – 400	280	$(4.21^{+0.27}_{-0.25} \ ^{+0.17}_{-0.18}) \cdot 10^{-2}$	$(2.25^{+0.23}_{-0.21} \ ^{+0.09}_{-0.10}) \cdot 10^{-2}$
400 – 711	530	$(3.19^{+0.16}_{-0.15} \ ^{+0.10}_{-0.10}) \cdot 10^{-2}$	$(1.25^{+0.12}_{-0.11} \ ^{+0.04}_{-0.04}) \cdot 10^{-2}$
711 – 1265	950	$(1.69^{+0.08}_{-0.08} \ ^{+0.03}_{-0.04}) \cdot 10^{-2}$	$(8.45^{+0.70}_{-0.65} \ ^{+0.17}_{-0.21}) \cdot 10^{-3}$
1265 – 2249	1700	$(8.87^{+0.43}_{-0.41} \ ^{+0.11}_{-0.14}) \cdot 10^{-3}$	$(4.18^{+0.36}_{-0.33} \ ^{+0.07}_{-0.06}) \cdot 10^{-3}$
2249 – 4000	3000	$(3.91^{+0.21}_{-0.20} \ ^{+0.10}_{-0.10}) \cdot 10^{-3}$	$(1.97^{+0.18}_{-0.17} \ ^{+0.06}_{-0.06}) \cdot 10^{-3}$
4000 – 7113	5300	$(1.30^{+0.09}_{-0.09} \ ^{+0.07}_{-0.07}) \cdot 10^{-3}$	$(6.81^{+0.82}_{-0.73} \ ^{+0.39}_{-0.38}) \cdot 10^{-4}$
7113 – 12469	9500	$(2.67^{+0.31}_{-0.28} \ ^{+0.30}_{-0.24}) \cdot 10^{-4}$	$(9.66^{+2.40}_{-1.96} \ ^{+1.10}_{-0.84}) \cdot 10^{-5}$
12469 – 22494	17000	$(3.17^{+0.79}_{-0.64} \ ^{+0.61}_{-0.50}) \cdot 10^{-5}$	$(1.80^{+0.77}_{-0.56} \ ^{+0.34}_{-0.28}) \cdot 10^{-5}$
22494 – 60000	30000	$(1.46^{+1.42}_{-0.79} \ ^{+0.48}_{-0.40}) \cdot 10^{-6}$	$(1.33^{+1.76}_{-0.86} \ ^{+0.44}_{-0.37}) \cdot 10^{-6}$
x range	x	$d\sigma/dx$ (pb)	
		$P_e = +0.33$	$P_e = -0.36$
0.006 – 0.010	0.0078	$(6.39^{+1.07}_{-0.93} \ ^{+0.42}_{-0.70}) \cdot 10^2$	$(3.64^{+0.98}_{-0.79} \ ^{+0.25}_{-0.36}) \cdot 10^2$
0.010 – 0.021	0.015	$(6.81^{+0.43}_{-0.40} \ ^{+0.26}_{-0.32}) \cdot 10^2$	$(3.32^{+0.36}_{-0.33} \ ^{+0.14}_{-0.15}) \cdot 10^2$
0.021 – 0.046	0.032	$(4.62^{+0.19}_{-0.19} \ ^{+0.09}_{-0.09}) \cdot 10^2$	$(1.98^{+0.15}_{-0.14} \ ^{+0.04}_{-0.04}) \cdot 10^2$
0.046 – 0.100	0.068	$(2.19^{+0.09}_{-0.08} \ ^{+0.03}_{-0.03}) \cdot 10^2$	$(1.07^{+0.07}_{-0.07} \ ^{+0.01}_{-0.02}) \cdot 10^2$
0.100 – 0.178	0.130	$(8.86^{+0.47}_{-0.45} \ ^{+0.20}_{-0.19}) \cdot 10^1$	$(4.87^{+0.42}_{-0.39} \ ^{+0.12}_{-0.11}) \cdot 10^1$
0.178 – 0.316	0.240	$(3.30^{+0.23}_{-0.22} \ ^{+0.14}_{-0.14}) \cdot 10^1$	$(1.49^{+0.19}_{-0.17} \ ^{+0.07}_{-0.07}) \cdot 10^1$
0.316 – 0.562	0.420	$(7.75^{+1.03}_{-0.92} \ ^{+0.70}_{-0.66}) \cdot 10^0$	$(2.83^{+0.81}_{-0.64} \ ^{+0.27}_{-0.23}) \cdot 10^0$
0.562 – 1.000	0.650	$(1.71^{+3.94}_{-1.42} \ ^{+0.58}_{-0.36}) \cdot 10^{-1}$	$(2.35^{+5.41}_{-1.95} \ ^{+0.58}_{-0.51}) \cdot 10^{-1}$
y range	y	$d\sigma/dy$ (pb)	
		$P_e = +0.33$	$P_e = -0.36$
0.00 – 0.10	0.05	$103.9^{+5.4}_{-5.1} \ ^{+1.5}_{-1.9}$	$56.2^{+4.7}_{-4.4} \ ^{+1.0}_{-1.1}$
0.10 – 0.20	0.15	$87.0^{+3.9}_{-3.7} \ ^{+0.9}_{-1.1}$	$39.6^{+3.1}_{-2.9} \ ^{+0.6}_{-0.6}$
0.20 – 0.34	0.27	$66.5^{+2.9}_{-2.8} \ ^{+0.9}_{-1.0}$	$31.9^{+2.4}_{-2.3} \ ^{+0.5}_{-0.5}$
0.34 – 0.48	0.41	$49.3^{+2.7}_{-2.6} \ ^{+0.9}_{-0.9}$	$20.5^{+2.1}_{-1.9} \ ^{+0.5}_{-0.4}$
0.48 – 0.62	0.55	$35.6^{+2.5}_{-2.3} \ ^{+0.9}_{-1.1}$	$18.5^{+2.2}_{-1.9} \ ^{+0.5}_{-0.6}$
0.62 – 0.76	0.69	$25.9^{+2.4}_{-2.2} \ ^{+1.1}_{-1.1}$	$11.1^{+1.9}_{-1.7} \ ^{+0.5}_{-0.5}$
0.76 – 0.90	0.83	$19.5^{+2.6}_{-2.3} \ ^{+1.5}_{-1.5}$	$10.5^{+2.4}_{-2.0} \ ^{+0.9}_{-0.9}$

Table 1: Values of the differential cross-sections $d\sigma/dQ^2$, $d\sigma/dx$ and $d\sigma/dy$ for $P_e = +0.33 \pm 0.01$ and $P_e = -0.36 \pm 0.01$. The following quantities are given: the range of the measurement; the value at which the cross section is quoted and the measured cross section, with statistical and systematic uncertainties.

$d\sigma/dQ^2 (P_e = +0.33 \pm 0.01)$						
Q^2 (GeV ²)	$d\sigma/dQ^2$ (pb/GeV ²)	δ_{stat} (%)	δ_{syst} (%)	δ_{unc} (%)	δ_{trk} (%)	δ_{es} (%)
280	$4.21 \cdot 10^{-2}$	+6.4 -6.0	+4.0 -4.4	+0.5 -2.0	+1.4 -1.4	+3.7 -3.6
530	$3.19 \cdot 10^{-2}$	+5.1 -4.8	+3.1 -3.0	+0.6 -1.2	+1.3 -1.3	+2.7 -2.4
950	$1.69 \cdot 10^{-2}$	+4.9 -4.7	+1.9 -2.4	+0.6 -1.6	+1.2 -1.1	+1.3 -1.3
1700	$8.87 \cdot 10^{-3}$	+4.9 -4.7	+1.3 -1.6	+0.6 -1.2	+1.1 -1.1	+0.3 -0.0
3000	$3.91 \cdot 10^{-3}$	+5.5 -5.2	+2.5 -2.7	+0.6 -1.0	+1.0 -1.0	-2.2 +2.3
5300	$1.30 \cdot 10^{-3}$	+7.1 -6.7	+5.6 -5.2	+0.8 -0.6	+1.0 -0.9	-5.1 +5.5
9500	$2.67 \cdot 10^{-4}$	+11.7 -10.5	+11.3 -8.8	+0.9 -1.9	+0.9 -0.9	-8.5 +11.2
17000	$3.17 \cdot 10^{-5}$	+24.9 -20.3	+19.3 -15.9	+0.0 -4.7	+0.9 -0.9	-15.1 +19.3
30000	$1.46 \cdot 10^{-6}$	+97.3 -54.4	+32.6 -27.4	+0.0 -5.6	+1.0 -1.0	-26.8 +32.6
$d\sigma/dx (P_e = +0.33 \pm 0.01)$						
x	$d\sigma/dx$ (pb)	δ_{stat} (%)	δ_{syst} (%)	δ_{unc} (%)	δ_{trk} (%)	δ_{es} (%)
0.0078	$6.39 \cdot 10^2$	+16.8 -14.5	+6.5 -10.9	+0.7 -9.2	+2.4 -2.3	+5.9 -5.4
0.015	$6.81 \cdot 10^2$	+6.3 -5.9	+3.8 -4.7	+0.6 -3.4	+2.0 -1.9	+3.2 -2.7
0.032	$4.62 \cdot 10^2$	+4.2 -4.0	+1.9 -2.0	+0.6 -0.8	+1.4 -1.4	+1.0 -1.2
0.068	$2.19 \cdot 10^2$	+3.9 -3.8	+1.2 -1.2	+0.5 -0.6	+1.0 -1.0	-0.3 +0.4
0.130	$8.86 \cdot 10^1$	+5.3 -5.1	+2.2 -2.1	+0.6 -0.9	+0.7 -0.7	-1.8 +2.0
0.240	$3.30 \cdot 10^1$	+7.1 -6.7	+4.2 -4.3	+0.4 -1.3	+0.5 -0.5	-4.1 +4.1
0.420	$7.75 \cdot 10^0$	+13.3 -11.8	+9.1 -8.5	+0.7 -2.7	+0.4 -0.4	-8.1 +9.0
0.650	$1.71 \cdot 10^{-1}$	+229.9 -82.7	+33.9 -20.8	+23.3 -3.2	+0.3 -0.3	-20.5 +24.6
$d\sigma/dy (P_e = +0.33 \pm 0.01)$						
y	$d\sigma/dy$ (pb)	δ_{stat} (%)	δ_{syst} (%)	δ_{unc} (%)	δ_{trk} (%)	δ_{es} (%)
0.05	103.9	+5.2 -4.9	+1.5 -1.8	+0.6 -1.0	+0.7 -0.6	+1.2 -1.4
0.15	87.0	+4.5 -4.3	+1.1 -1.2	+0.5 -0.8	+0.8 -0.8	+0.4 -0.4
0.27	66.5	+4.4 -4.2	+1.3 -1.5	+0.7 -1.0	+1.1 -1.1	-0.0 +0.1
0.41	49.3	+5.5 -5.2	+1.8 -1.8	+0.3 -0.8	+1.4 -1.4	-0.9 +1.1
0.55	35.6	+7.0 -6.5	+2.5 -3.1	+0.5 -2.0	+1.6 -1.5	-1.8 +1.8
0.69	25.9	+9.2 -8.5	+4.1 -4.4	+0.8 -2.8	+1.8 -1.8	-2.9 +3.6
0.83	19.5	+13.3 -11.8	+7.7 -7.8	+0.3 -3.3	+1.9 -1.8	-6.8 +7.4

Table 2: Values of the differential cross-sections $d\sigma/dQ^2$, $d\sigma/dx$ and $d\sigma/dy$ for $P_e = +0.33 \pm 0.01$. The following quantities are given: the value at which the cross section is quoted; the measured cross section; the statistical uncertainty; the total systematic uncertainty (δ_{syst}); the uncorrelated systematic uncertainty (δ_{unc}); the uncertainty on FLT tracking efficiency (δ_{trk}) and the calorimeter energy-scale uncertainty (δ_{es}). Both δ_{trk} and δ_{es} have significant correlations between cross-section bins.

$d\sigma/dQ^2 (P_e = -0.36 \pm 0.01)$						
Q^2 (GeV ²)	$d\sigma/dQ^2$ (pb/GeV ²)	δ_{stat} (%)	δ_{syst} (%)	δ_{unc} (%)	δ_{trk} (%)	δ_{es} (%)
280	$2.25 \cdot 10^{-2}$	+10.3 -9.4	+4.1 -4.5	+0.6 -2.0	+1.7 -1.7	+3.7 -3.7
530	$1.25 \cdot 10^{-2}$	+9.8 -9.0	+3.2 -3.0	+0.7 -0.8	+1.6 -1.5	+2.7 -2.5
950	$8.45 \cdot 10^{-3}$	+8.3 -7.7	+2.0 -2.4	+0.4 -1.5	+1.4 -1.4	+1.3 -1.3
1700	$4.18 \cdot 10^{-3}$	+8.6 -7.9	+1.6 -1.5	+0.8 -0.8	+1.3 -1.3	+0.3 -0.0
3000	$1.97 \cdot 10^{-3}$	+9.3 -8.5	+2.8 -2.8	+1.1 -1.3	+1.2 -1.2	-2.2 +2.3
5300	$6.81 \cdot 10^{-4}$	+12.0 -10.8	+5.7 -5.6	+0.7 -2.1	+1.1 -1.1	-5.1 +5.5
9500	$9.66 \cdot 10^{-5}$	+24.9 -20.2	+11.4 -8.7	+1.8 -0.9	+1.1 -1.1	-8.6 +11.2
17000	$1.80 \cdot 10^{-5}$	+42.7 -31.0	+19.2 -15.8	+0.0 -4.7	+1.1 -1.1	-15.1 +19.2
30000	$1.33 \cdot 10^{-6}$	+131.9 -64.6	+32.8 -27.4	+0.0 -5.5	+1.2 -1.2	-26.8 +32.8
$d\sigma/dx (P_e = -0.36 \pm 0.01)$						
x	$d\sigma/dx$ (pb)	δ_{stat} (%)	δ_{syst} (%)	δ_{unc} (%)	δ_{trk} (%)	δ_{es} (%)
0.0078	$3.64 \cdot 10^2$	+26.9 -21.6	+6.9 -10.0	+0.7 -7.9	+3.1 -3.0	+5.9 -5.4
0.015	$3.32 \cdot 10^2$	+10.8 -9.8	+4.1 -4.5	+1.1 -2.8	+2.4 -2.3	+3.2 -2.7
0.032	$1.98 \cdot 10^2$	+7.7 -7.2	+2.1 -2.2	+0.5 -0.8	+1.7 -1.7	+1.1 -1.2
0.068	$1.07 \cdot 10^2$	+6.7 -6.3	+1.4 -1.5	+0.5 -0.8	+1.2 -1.2	-0.3 +0.4
0.130	$4.87 \cdot 10^1$	+8.6 -8.0	+2.4 -2.3	+0.8 -1.2	+0.9 -0.9	-1.8 +2.0
0.240	$1.49 \cdot 10^1$	+12.9 -11.5	+4.8 -4.4	+2.2 -1.6	+0.7 -0.7	-4.1 +4.1
0.420	$2.83 \cdot 10^0$	+28.6 -22.7	+9.7 -8.3	+3.6 -1.7	+0.5 -0.5	-8.1 +9.0
0.650	$2.35 \cdot 10^{-1}$	+229.9 -82.7	+24.5 -21.8	+0.0 -7.6	+0.4 -0.4	-20.4 +24.5
$d\sigma/dy (P_e = -0.36 \pm 0.01)$						
y	$d\sigma/dy$ (pb)	δ_{stat} (%)	δ_{syst} (%)	δ_{unc} (%)	δ_{trk} (%)	δ_{es} (%)
0.05	56.2	+8.4 -7.8	+1.7 -2.0	+0.9 -1.2	+0.9 -0.9	+1.2 -1.4
0.15	39.6	+7.9 -7.4	+1.5 -1.4	+0.9 -0.8	+1.1 -1.1	+0.4 -0.5
0.27	31.9	+7.6 -7.1	+1.5 -1.6	+0.7 -0.8	+1.4 -1.3	-0.0 +0.1
0.41	20.5	+10.3 -9.4	+2.3 -2.1	+1.3 -1.0	+1.6 -1.6	-0.9 +1.1
0.55	18.5	+11.7 -10.5	+2.6 -3.0	+0.3 -1.7	+1.8 -1.8	-1.8 +1.9
0.69	11.1	+17.5 -15.0	+4.3 -4.9	+0.9 -3.4	+2.2 -2.1	-2.9 +3.6
0.83	10.5	+22.7 -18.8	+8.2 -8.3	+1.9 -3.9	+2.5 -2.4	-6.9 +7.6

Table 3: Values of the differential cross-sections $d\sigma/dQ^2$, $d\sigma/dx$ and $d\sigma/dy$ for $P_e = -0.36 \pm 0.01$. The following quantities are given: the value at which the cross section is quoted; the measured cross section; the statistical uncertainty; the total systematic uncertainty (δ_{syst}); the uncorrelated systematic uncertainty (δ_{unc}); the uncertainty on FLT tracking efficiency (δ_{trk}) and the calorimeter energy-scale uncertainty (δ_{es}). Both δ_{trk} and δ_{es} have significant correlations between cross-section bins.

Q^2 (GeV ²)	x	$\tilde{\sigma}$		
		$P_e = -0.36$	$P_e = +0.33$	$P_e = 0$
280	0.0078	$(8.23^{+2.84}_{-2.18} \ ^{+0.59}_{-0.76}) \cdot 10^{-1}$	$(1.44^{+0.31}_{-0.26} \ ^{+0.10}_{-0.12}) \cdot 10^0$	$(1.14^{+0.20}_{-0.17} \ ^{+0.08}_{-0.10}) \cdot 10^0$
280	0.015	$(9.07^{+1.72}_{-1.47} \ ^{+0.49}_{-0.51}) \cdot 10^{-1}$	$(1.85^{+0.20}_{-0.18} \ ^{+0.10}_{-0.11}) \cdot 10^0$	$(1.40^{+0.13}_{-0.12} \ ^{+0.07}_{-0.08}) \cdot 10^0$
280	0.032	$(6.39^{+1.27}_{-1.08} \ ^{+0.19}_{-0.22}) \cdot 10^{-1}$	$(1.12^{+0.14}_{-0.12} \ ^{+0.03}_{-0.04}) \cdot 10^0$	$(8.84^{+0.89}_{-0.81} \ ^{+0.26}_{-0.30}) \cdot 10^{-1}$
280	0.068	$(3.91^{+1.08}_{-0.87} \ ^{+0.11}_{-0.14}) \cdot 10^{-1}$	$(7.03^{+1.17}_{-1.01} \ ^{+0.20}_{-0.26}) \cdot 10^{-1}$	$(5.52^{+0.75}_{-0.67} \ ^{+0.16}_{-0.20}) \cdot 10^{-1}$
280	0.130	$(3.27^{+2.58}_{-1.56} \ ^{+0.12}_{-0.12}) \cdot 10^{-1}$	$(7.88^{+2.85}_{-2.16} \ ^{+0.26}_{-0.28}) \cdot 10^{-1}$	$(5.74^{+1.76}_{-1.38} \ ^{+0.19}_{-0.21}) \cdot 10^{-1}$
530	0.0078	$(4.86^{+2.90}_{-1.93} \ ^{+0.38}_{-0.56}) \cdot 10^{-1}$	$(9.61^{+3.18}_{-2.45} \ ^{+0.62}_{-1.35}) \cdot 10^{-1}$	$(7.37^{+1.98}_{-1.59} \ ^{+0.50}_{-0.95}) \cdot 10^{-1}$
530	0.015	$(6.19^{+1.25}_{-1.06} \ ^{+0.24}_{-0.22}) \cdot 10^{-1}$	$(1.32^{+0.15}_{-0.13} \ ^{+0.05}_{-0.05}) \cdot 10^0$	$(9.90^{+0.93}_{-0.86} \ ^{+0.37}_{-0.35}) \cdot 10^{-1}$
530	0.032	$(4.63^{+0.89}_{-0.76} \ ^{+0.12}_{-0.12}) \cdot 10^{-1}$	$(1.55^{+0.13}_{-0.12} \ ^{+0.04}_{-0.04}) \cdot 10^0$	$(1.05^{+0.08}_{-0.07} \ ^{+0.03}_{-0.02}) \cdot 10^0$
530	0.068	$(4.61^{+0.86}_{-0.74} \ ^{+0.14}_{-0.11}) \cdot 10^{-1}$	$(9.04^{+0.98}_{-0.89} \ ^{+0.27}_{-0.21}) \cdot 10^{-1}$	$(6.93^{+0.63}_{-0.58} \ ^{+0.21}_{-0.16}) \cdot 10^{-1}$
530	0.130	$(1.64^{+0.81}_{-0.57} \ ^{+0.04}_{-0.04}) \cdot 10^{-1}$	$(5.52^{+1.08}_{-0.92} \ ^{+0.14}_{-0.12}) \cdot 10^{-1}$	$(3.75^{+0.65}_{-0.56} \ ^{+0.10}_{-0.08}) \cdot 10^{-1}$
950	0.015	$(3.98^{+0.99}_{-0.81} \ ^{+0.15}_{-0.24}) \cdot 10^{-1}$	$(9.15^{+1.18}_{-1.05} \ ^{+0.26}_{-0.50}) \cdot 10^{-1}$	$(6.73^{+0.75}_{-0.68} \ ^{+0.20}_{-0.37}) \cdot 10^{-1}$
950	0.032	$(4.30^{+0.69}_{-0.60} \ ^{+0.10}_{-0.12}) \cdot 10^{-1}$	$(1.04^{+0.09}_{-0.08} \ ^{+0.02}_{-0.03}) \cdot 10^0$	$(7.57^{+0.55}_{-0.51} \ ^{+0.17}_{-0.20}) \cdot 10^{-1}$
950	0.068	$(4.37^{+0.66}_{-0.58} \ ^{+0.07}_{-0.08}) \cdot 10^{-1}$	$(6.75^{+0.67}_{-0.62} \ ^{+0.10}_{-0.10}) \cdot 10^{-1}$	$(5.55^{+0.45}_{-0.42} \ ^{+0.09}_{-0.08}) \cdot 10^{-1}$
950	0.130	$(3.04^{+0.69}_{-0.57} \ ^{+0.05}_{-0.06}) \cdot 10^{-1}$	$(5.98^{+0.77}_{-0.69} \ ^{+0.10}_{-0.11}) \cdot 10^{-1}$	$(4.58^{+0.50}_{-0.45} \ ^{+0.07}_{-0.08}) \cdot 10^{-1}$
950	0.240	$(1.12^{+0.67}_{-0.44} \ ^{+0.01}_{-0.01}) \cdot 10^{-1}$	$(2.31^{+0.71}_{-0.56} \ ^{+0.01}_{-0.02}) \cdot 10^{-1}$	$(1.75^{+0.45}_{-0.36} \ ^{+0.01}_{-0.01}) \cdot 10^{-1}$
1700	0.032	$(3.12^{+0.52}_{-0.45} \ ^{+0.09}_{-0.07}) \cdot 10^{-1}$	$(7.20^{+0.64}_{-0.59} \ ^{+0.13}_{-0.18}) \cdot 10^{-1}$	$(5.29^{+0.41}_{-0.38} \ ^{+0.10}_{-0.11}) \cdot 10^{-1}$
1700	0.068	$(2.48^{+0.42}_{-0.36} \ ^{+0.03}_{-0.04}) \cdot 10^{-1}$	$(7.10^{+0.57}_{-0.53} \ ^{+0.09}_{-0.10}) \cdot 10^{-1}$	$(4.98^{+0.35}_{-0.33} \ ^{+0.06}_{-0.06}) \cdot 10^{-1}$
1700	0.130	$(2.68^{+0.52}_{-0.44} \ ^{+0.03}_{-0.04}) \cdot 10^{-1}$	$(3.66^{+0.50}_{-0.45} \ ^{+0.04}_{-0.03}) \cdot 10^{-1}$	$(3.14^{+0.34}_{-0.31} \ ^{+0.03}_{-0.03}) \cdot 10^{-1}$
1700	0.240	$(1.65^{+0.46}_{-0.37} \ ^{+0.05}_{-0.03}) \cdot 10^{-1}$	$(2.66^{+0.46}_{-0.40} \ ^{+0.02}_{-0.04}) \cdot 10^{-1}$	$(2.16^{+0.30}_{-0.27} \ ^{+0.03}_{-0.03}) \cdot 10^{-1}$
1700	0.420	$(1.80^{+4.14}_{-1.49} \ ^{+0.08}_{-0.08}) \cdot 10^{-2}$	$(9.47^{+5.10}_{-3.49} \ ^{+0.32}_{-0.44}) \cdot 10^{-2}$	$(6.03^{+2.97}_{-2.09} \ ^{+0.22}_{-0.27}) \cdot 10^{-2}$
3000	0.032	$(3.10^{+0.79}_{-0.64} \ ^{+0.14}_{-0.19}) \cdot 10^{-1}$	$(4.73^{+0.79}_{-0.68} \ ^{+0.23}_{-0.17}) \cdot 10^{-1}$	$(3.91^{+0.52}_{-0.46} \ ^{+0.18}_{-0.15}) \cdot 10^{-1}$
3000	0.068	$(2.47^{+0.38}_{-0.33} \ ^{+0.06}_{-0.08}) \cdot 10^{-1}$	$(5.24^{+0.44}_{-0.41} \ ^{+0.12}_{-0.15}) \cdot 10^{-1}$	$(3.93^{+0.28}_{-0.27} \ ^{+0.09}_{-0.12}) \cdot 10^{-1}$
3000	0.130	$(2.08^{+0.39}_{-0.34} \ ^{+0.05}_{-0.03}) \cdot 10^{-1}$	$(3.41^{+0.41}_{-0.37} \ ^{+0.07}_{-0.05}) \cdot 10^{-1}$	$(2.75^{+0.27}_{-0.25} \ ^{+0.06}_{-0.04}) \cdot 10^{-1}$
3000	0.240	$(9.08^{+2.87}_{-2.25} \ ^{+0.51}_{-0.31}) \cdot 10^{-2}$	$(2.63^{+0.37}_{-0.33} \ ^{+0.07}_{-0.07}) \cdot 10^{-1}$	$(1.84^{+0.23}_{-0.21} \ ^{+0.06}_{-0.05}) \cdot 10^{-1}$
3000	0.420	$(2.95^{+2.33}_{-1.41} \ ^{+0.12}_{-0.20}) \cdot 10^{-2}$	$(6.47^{+2.46}_{-1.84} \ ^{+0.26}_{-0.39}) \cdot 10^{-2}$	$(4.82^{+1.53}_{-1.19} \ ^{+0.18}_{-0.30}) \cdot 10^{-2}$
5300	0.068	$(1.68^{+0.37}_{-0.31} \ ^{+0.10}_{-0.10}) \cdot 10^{-1}$	$(3.05^{+0.40}_{-0.35} \ ^{+0.19}_{-0.16}) \cdot 10^{-1}$	$(2.39^{+0.26}_{-0.23} \ ^{+0.15}_{-0.13}) \cdot 10^{-1}$
5300	0.130	$(1.55^{+0.33}_{-0.27} \ ^{+0.08}_{-0.08}) \cdot 10^{-1}$	$(2.45^{+0.33}_{-0.29} \ ^{+0.12}_{-0.12}) \cdot 10^{-1}$	$(2.00^{+0.22}_{-0.20} \ ^{+0.10}_{-0.10}) \cdot 10^{-1}$
5300	0.240	$(9.97^{+2.76}_{-2.21} \ ^{+0.53}_{-0.57}) \cdot 10^{-2}$	$(1.83^{+0.30}_{-0.26} \ ^{+0.10}_{-0.10}) \cdot 10^{-1}$	$(1.43^{+0.19}_{-0.17} \ ^{+0.07}_{-0.08}) \cdot 10^{-1}$
5300	0.420	$(2.12^{+1.67}_{-1.01} \ ^{+0.22}_{-0.13}) \cdot 10^{-2}$	$(1.17^{+0.25}_{-0.21} \ ^{+0.11}_{-0.08}) \cdot 10^{-1}$	$(7.39^{+1.50}_{-1.26} \ ^{+0.68}_{-0.48}) \cdot 10^{-2}$
9500	0.130	$(4.54^{+2.07}_{-1.48} \ ^{+0.56}_{-0.45}) \cdot 10^{-2}$	$(1.42^{+0.27}_{-0.23} \ ^{+0.18}_{-0.14}) \cdot 10^{-1}$	$(9.79^{+1.64}_{-1.42} \ ^{+1.21}_{-0.97}) \cdot 10^{-2}$
9500	0.240	$(3.50^{+1.89}_{-1.29} \ ^{+0.39}_{-0.26}) \cdot 10^{-2}$	$(1.33^{+0.26}_{-0.22} \ ^{+0.13}_{-0.10}) \cdot 10^{-1}$	$(8.84^{+1.56}_{-1.34} \ ^{+0.84}_{-0.65}) \cdot 10^{-2}$
9500	0.420	$(3.66^{+1.97}_{-1.35} \ ^{+0.59}_{-0.37}) \cdot 10^{-2}$	$(4.20^{+1.69}_{-1.25} \ ^{+0.48}_{-0.43}) \cdot 10^{-2}$	$(3.84^{+1.14}_{-0.90} \ ^{+0.43}_{-0.38}) \cdot 10^{-2}$
17000	0.240	$(3.02^{+1.80}_{-1.20} \ ^{+0.57}_{-0.46}) \cdot 10^{-2}$	$(3.69^{+1.58}_{-1.14} \ ^{+0.70}_{-0.57}) \cdot 10^{-2}$	$(3.29^{+1.04}_{-0.82} \ ^{+0.63}_{-0.51}) \cdot 10^{-2}$
17000	0.420	$(1.10^{+1.45}_{-0.71} \ ^{+0.19}_{-0.14}) \cdot 10^{-2}$	$(3.21^{+1.58}_{-1.11} \ ^{+0.57}_{-0.42}) \cdot 10^{-2}$	$(2.24^{+0.96}_{-0.70} \ ^{+0.43}_{-0.29}) \cdot 10^{-2}$
30000	0.420	$(5.32^{+12.24}_{-4.41} \ ^{+1.85}_{-1.47}) \cdot 10^{-3}$	$(1.17^{+1.14}_{-0.64} \ ^{+0.41}_{-0.32}) \cdot 10^{-2}$	$(8.71^{+6.89}_{-4.17} \ ^{+3.03}_{-2.40}) \cdot 10^{-3}$

Table 4: Values of the reduced cross section. The following quantities are given: the values of Q^2 and x at which the cross section is quoted and the measured cross section, with statistical and systematic uncertainties.

Q^2 (GeV ²)	x	$\tilde{\sigma}$	δ_{stat} (%)	δ_{syst} (%)	δ_{unc} (%)	δ_{trk} (%)	δ_{es} (%)
280	0.0078	$1.44 \cdot 10^0$	+21.4 -17.9	+7.0 -8.3	+0.5 -7.0	+2.3 -2.2	+6.5 -3.9
280	0.015	$1.85 \cdot 10^0$	+10.9 -9.9	+5.1 -5.7	+0.6 -3.2	+1.9 -1.9	+4.7 -4.4
280	0.032	$1.12 \cdot 10^0$	+12.2 -11.0	+2.9 -3.3	+0.6 -0.4	+1.1 -1.1	+2.6 -3.1
280	0.068	$7.03 \cdot 10^{-1}$	+16.6 -14.4	+2.8 -3.6	+0.5 -1.0	+0.8 -0.8	+2.7 -3.4
280	0.130	$7.88 \cdot 10^{-1}$	+36.2 -27.4	+3.3 -3.6	+0.5 -2.2	+0.5 -0.5	+3.2 -2.8
530	0.0078	$9.61 \cdot 10^{-1}$	+33.1 -25.5	+6.4 -14.1	+0.9 -11.9	+2.6 -2.4	+5.7 -7.1
530	0.015	$1.32 \cdot 10^0$	+11.1 -10.0	+3.7 -3.7	+0.5 -1.7	+2.0 -1.9	+3.0 -2.7
530	0.032	$1.55 \cdot 10^0$	+8.3 -7.7	+2.5 -2.3	+0.6 -0.4	+1.2 -1.2	+2.0 -1.9
530	0.068	$9.04 \cdot 10^{-1}$	+10.8 -9.9	+3.0 -2.3	+0.7 -0.4	+0.8 -0.8	+2.8 -2.1
530	0.130	$5.52 \cdot 10^{-1}$	+19.6 -16.6	+2.6 -2.2	+0.8 -1.1	+0.6 -0.6	+2.4 -1.8
950	0.015	$9.15 \cdot 10^{-1}$	+12.9 -11.5	+2.9 -5.5	+0.7 -4.9	+2.0 -1.9	+1.9 -1.3
950	0.032	$1.04 \cdot 10^0$	+8.3 -7.7	+2.3 -2.6	+0.6 -1.3	+1.4 -1.4	+1.6 -1.8
950	0.068	$6.75 \cdot 10^{-1}$	+10.0 -9.1	+1.5 -1.4	+0.6 -0.9	+0.9 -0.8	+1.1 -0.7
950	0.130	$5.98 \cdot 10^{-1}$	+12.9 -11.5	+1.7 -1.8	+1.3 -1.1	+0.5 -0.5	+0.9 -1.3
950	0.240	$2.31 \cdot 10^{-1}$	+30.6 -24.1	+0.4 -0.7	+0.0 -0.0	+0.4 -0.4	-0.0 -0.6
1700	0.032	$7.20 \cdot 10^{-1}$	+8.9 -8.2	+1.8 -2.4	+0.5 -1.7	+1.7 -1.6	+0.2 -0.5
1700	0.068	$7.10 \cdot 10^{-1}$	+8.0 -7.4	+1.2 -1.5	+0.7 -1.1	+0.9 -0.9	+0.3 +0.2
1700	0.130	$3.66 \cdot 10^{-1}$	+13.8 -12.2	+1.1 -0.9	+0.6 -0.7	+0.6 -0.6	+0.6 +0.2
1700	0.240	$2.66 \cdot 10^{-1}$	+17.5 -15.0	+0.8 -1.6	+0.4 -1.4	+0.5 -0.5	-0.7 +0.5
1700	0.420	$9.47 \cdot 10^{-2}$	+53.9 -36.8	+3.4 -4.7	+2.0 -4.5	+0.2 -0.2	-1.2 +2.7
3000	0.032	$4.73 \cdot 10^{-1}$	+16.6 -14.4	+4.8 -3.6	+1.8 -1.6	+1.8 -1.8	-2.8 +4.1
3000	0.068	$5.24 \cdot 10^{-1}$	+8.5 -7.9	+2.2 -2.9	+0.4 -0.8	+1.2 -1.2	-2.6 +1.8
3000	0.130	$3.41 \cdot 10^{-1}$	+12.1 -10.8	+2.0 -1.5	+1.0 -0.9	+0.7 -0.7	-1.0 +1.6
3000	0.240	$2.63 \cdot 10^{-1}$	+14.3 -12.6	+2.6 -2.8	+0.4 -1.7	+0.4 -0.4	-2.2 +2.5
3000	0.420	$6.47 \cdot 10^{-2}$	+38.0 -28.4	+4.0 -6.0	+1.7 -2.3	+0.3 -0.3	-5.5 +3.6
5300	0.068	$3.05 \cdot 10^{-1}$	+13.0 -11.6	+6.2 -5.3	+1.0 -1.1	+1.6 -1.5	-4.9 +6.0
5300	0.130	$2.45 \cdot 10^{-1}$	+13.6 -12.0	+5.0 -4.9	+0.8 -0.8	+0.8 -0.8	-4.8 +4.9
5300	0.240	$1.83 \cdot 10^{-1}$	+16.2 -14.1	+5.2 -5.5	+2.0 -1.0	+0.6 -0.6	-5.4 +4.8
5300	0.420	$1.17 \cdot 10^{-1}$	+21.8 -18.2	+9.2 -7.0	+2.3 -3.9	+0.4 -0.4	-5.8 +8.9
9500	0.130	$1.42 \cdot 10^{-1}$	+19.0 -16.2	+12.6 -10.0	+2.5 -3.4	+1.3 -1.3	-9.3 +12.3
9500	0.240	$1.33 \cdot 10^{-1}$	+19.6 -16.6	+9.5 -7.5	+0.6 -2.1	+0.7 -0.7	-7.2 +9.5
9500	0.420	$4.20 \cdot 10^{-2}$	+40.1 -29.7	+11.3 -10.2	+3.2 -2.5	+0.4 -0.4	-9.8 +10.9
17000	0.240	$3.69 \cdot 10^{-2}$	+42.7 -31.0	+19.0 -15.4	+0.0 -4.8	+1.0 -1.0	-14.6 +18.9
17000	0.420	$3.21 \cdot 10^{-2}$	+49.3 -34.6	+17.7 -12.9	+0.0 -3.5	+0.6 -0.5	-12.4 +17.7
30000	0.420	$1.17 \cdot 10^{-2}$	+97.3 -54.4	+34.8 -27.5	+0.0 -4.8	+0.9 -0.9	-27.1 +34.8

Table 5: Values of the reduced cross section for $P_e = +0.33 \pm 0.01$. The following quantities are given: the values of Q^2 and x at which the cross section is quoted; the measured cross section; the statistical uncertainty; the total systematic uncertainty (δ_{syst}); the uncorrelated systematic uncertainty (δ_{unc}); the uncertainty on FLT tracking efficiency (δ_{trk}) and the calorimeter energy-scale uncertainty (δ_{es}). Both δ_{trk} and δ_{es} have significant correlations between cross-section bins.

Q^2 (GeV ²)	x	$\bar{\sigma}$	δ_{stat} (%)	δ_{syst} (%)	δ_{unc} (%)	δ_{trk} (%)	δ_{es} (%)
280	0.0078	$8.23 \cdot 10^{-1}$	+34.5 -26.4	+7.2 -9.2	+0.9 -7.8	+2.9 -2.7	+6.2 -4.0
280	0.015	$9.07 \cdot 10^{-1}$	+19.0 -16.2	+5.3 -5.7	+0.5 -2.7	+2.3 -2.2	+4.7 -4.4
280	0.032	$6.39 \cdot 10^{-1}$	+19.9 -16.8	+3.0 -3.5	+0.6 -0.6	+1.4 -1.4	+2.6 -3.1
280	0.068	$3.91 \cdot 10^{-1}$	+27.7 -22.1	+2.9 -3.7	+0.7 -0.9	+1.1 -1.0	+2.6 -3.4
280	0.130	$3.27 \cdot 10^{-1}$	+79.1 -47.9	+3.7 -3.7	+1.5 -2.4	+0.7 -0.7	+3.2 -2.7
530	0.0078	$4.86 \cdot 10^{-1}$	+59.7 -39.6	+7.7 -11.5	+2.4 -8.2	+3.7 -3.4	+6.1 -7.3
530	0.015	$6.19 \cdot 10^{-1}$	+20.3 -17.1	+3.8 -3.5	+0.6 -0.5	+2.2 -2.1	+3.0 -2.7
530	0.032	$4.63 \cdot 10^{-1}$	+19.3 -16.4	+2.7 -2.5	+0.9 -0.6	+1.5 -1.4	+2.0 -2.0
530	0.068	$4.61 \cdot 10^{-1}$	+18.7 -15.9	+3.1 -2.5	+0.5 -0.7	+1.0 -1.0	+2.8 -2.1
530	0.130	$1.64 \cdot 10^{-1}$	+49.3 -34.6	+2.7 -2.4	+0.9 -1.3	+0.8 -0.8	+2.4 -1.8
950	0.015	$3.98 \cdot 10^{-1}$	+24.9 -20.3	+3.9 -6.0	+2.3 -5.4	+2.5 -2.4	+1.8 -1.3
950	0.032	$4.30 \cdot 10^{-1}$	+16.1 -14.0	+2.3 -2.7	+0.2 -1.3	+1.7 -1.6	+1.6 -1.8
950	0.068	$4.37 \cdot 10^{-1}$	+15.1 -13.2	+1.6 -1.7	+0.4 -1.2	+1.1 -1.1	+1.2 -0.7
950	0.130	$3.04 \cdot 10^{-1}$	+22.7 -18.8	+1.6 -2.0	+1.1 -1.4	+0.7 -0.7	+0.9 -1.3
950	0.240	$1.12 \cdot 10^{-1}$	+59.7 -39.6	+0.6 -0.9	+0.0 -0.0	+0.6 -0.6	-0.0 -0.7
1700	0.032	$3.12 \cdot 10^{-1}$	+16.8 -14.5	+2.9 -2.2	+2.1 -1.1	+2.0 -1.9	+0.3 -0.5
1700	0.068	$2.48 \cdot 10^{-1}$	+16.8 -14.5	+1.3 -1.4	+0.5 -0.9	+1.1 -1.1	+0.3 +0.2
1700	0.130	$2.68 \cdot 10^{-1}$	+19.6 -16.6	+1.3 -1.6	+0.8 -1.4	+0.8 -0.8	+0.6 +0.2
1700	0.240	$1.65 \cdot 10^{-1}$	+27.7 -22.1	+3.0 -1.8	+2.9 -1.6	+0.6 -0.6	-0.7 +0.5
1700	0.420	$1.80 \cdot 10^{-2}$	+229.9 -82.7	+4.5 -4.2	+3.4 -4.0	+0.3 -0.3	-1.1 +2.9
3000	0.032	$3.10 \cdot 10^{-1}$	+25.5 -20.7	+4.6 -6.0	+0.3 -4.9	+2.2 -2.1	-2.7 +4.1
3000	0.068	$2.47 \cdot 10^{-1}$	+15.2 -13.3	+2.5 -3.1	+1.1 -1.1	+1.4 -1.4	-2.5 +1.8
3000	0.130	$2.08 \cdot 10^{-1}$	+19.0 -16.2	+2.6 -1.6	+1.9 -0.9	+0.9 -0.9	-1.0 +1.6
3000	0.240	$9.08 \cdot 10^{-2}$	+31.6 -24.7	+5.6 -3.4	+5.0 -2.5	+0.6 -0.6	-2.2 +2.5
3000	0.420	$2.95 \cdot 10^{-2}$	+79.1 -47.8	+3.9 -6.8	+1.7 -3.7	+0.5 -0.5	-5.6 +3.5
5300	0.068	$1.68 \cdot 10^{-1}$	+21.8 -18.2	+6.2 -6.1	+0.5 -3.2	+1.7 -1.6	-4.9 +6.0
5300	0.130	$1.55 \cdot 10^{-1}$	+21.0 -17.6	+5.1 -5.3	+0.8 -2.1	+1.0 -1.0	-4.8 +4.9
5300	0.240	$9.97 \cdot 10^{-2}$	+27.7 -22.2	+5.3 -5.7	+2.2 -1.6	+0.7 -0.7	-5.4 +4.8
5300	0.420	$2.12 \cdot 10^{-2}$	+79.1 -47.9	+10.5 -6.3	+5.6 -2.6	+0.5 -0.5	-5.7 +8.9
9500	0.130	$4.54 \cdot 10^{-2}$	+45.7 -32.7	+12.3 -10.0	+0.0 -3.0	+1.5 -1.5	-9.4 +12.3
9500	0.240	$3.50 \cdot 10^{-2}$	+53.9 -36.8	+11.1 -7.6	+5.6 -2.2	+0.8 -0.8	-7.2 +9.5
9500	0.420	$3.66 \cdot 10^{-2}$	+53.9 -36.8	+16.1 -10.1	+11.9 -2.4	+0.5 -0.5	-9.8 +10.8
17000	0.240	$3.02 \cdot 10^{-2}$	+59.7 -39.6	+19.0 -15.3	+0.0 -4.7	+1.2 -1.1	-14.5 +19.0
17000	0.420	$1.10 \cdot 10^{-2}$	+131.8 -64.6	+17.6 -12.9	+0.0 -3.5	+0.7 -0.7	-12.4 +17.6
30000	0.420	$5.32 \cdot 10^{-3}$	+229.9 -82.7	+34.7 -27.6	+0.0 -4.7	+1.2 -1.1	-27.2 +34.7

Table 6: Values of the reduced cross section for $P_e = -0.36 \pm 0.01$. The following quantities are given: the values of Q^2 and x at which the cross section is quoted; the measured cross section; the statistical uncertainty; the total systematic uncertainty (δ_{syst}); the uncorrelated systematic uncertainty (δ_{unc}); the uncertainty on FLT tracking efficiency (δ_{trk}) and the calorimeter energy-scale uncertainty (δ_{es}). Both δ_{trk} and δ_{es} have significant correlations between cross-section bins.

Polarisation	σ^{CC} (pb)
-0.413 ± 0.016	$20.7^{+1.4}_{-1.3}$ (stat.) ± 0.5 (lumi.) $^{+0.3}_{-0.4}$ (syst.)
-0.366 ± 0.015	$22.5^{+1.5}_{-1.4}$ (stat.) ± 0.6 (lumi.) $^{+0.4}_{-0.4}$ (syst.)
-0.306 ± 0.012	$25.1^{+1.5}_{-1.5}$ (stat.) ± 0.7 (lumi.) $^{+0.4}_{-0.4}$ (syst.)
0.259 ± 0.010	$46.4^{+2.0}_{-1.9}$ (stat.) ± 1.2 (lumi.) $^{+0.6}_{-0.7}$ (syst.)
0.303 ± 0.011	$46.7^{+2.0}_{-2.0}$ (stat.) ± 1.2 (lumi.) $^{+0.6}_{-0.8}$ (syst.)
0.339 ± 0.013	$48.4^{+2.1}_{-2.0}$ (stat.) ± 1.3 (lumi.) $^{+0.6}_{-0.8}$ (syst.)
0.416 ± 0.015	$51.4^{+2.1}_{-2.1}$ (stat.) ± 1.3 (lumi.) $^{+0.7}_{-0.8}$ (syst.)

Table 7: Values of the total cross section, σ^{CC} , measured at different values of polarisation of the positron beam. The following quantities are given: the polarisation value at which the cross section is quoted and the measured cross section, with statistical, luminosity and systematic uncertainties.

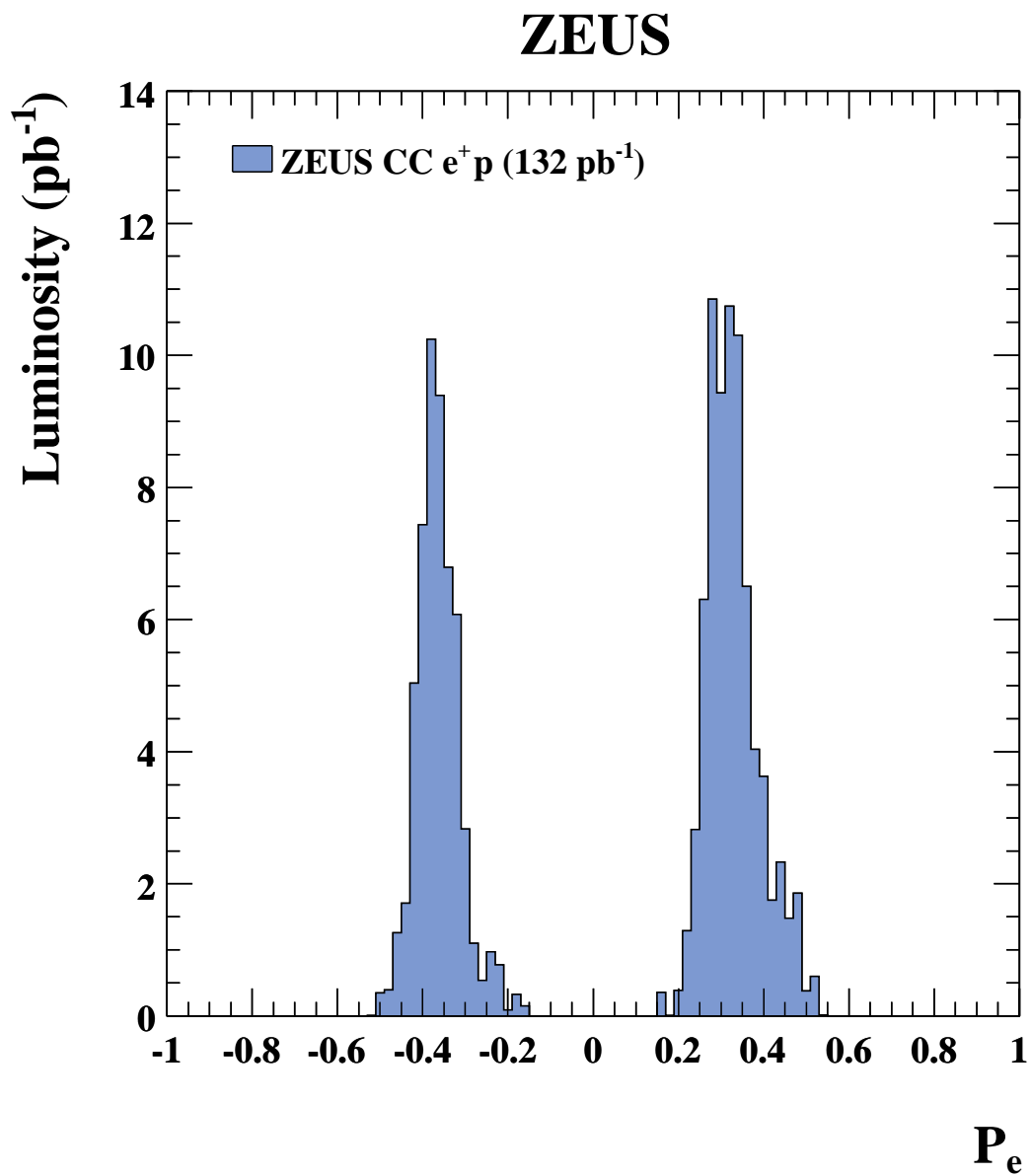


Figure 1: *The integrated luminosity collected as a function of the longitudinal polarisation of the positron beam. Events from runs with mean absolute polarisation less than 15% were rejected.*

ZEUS

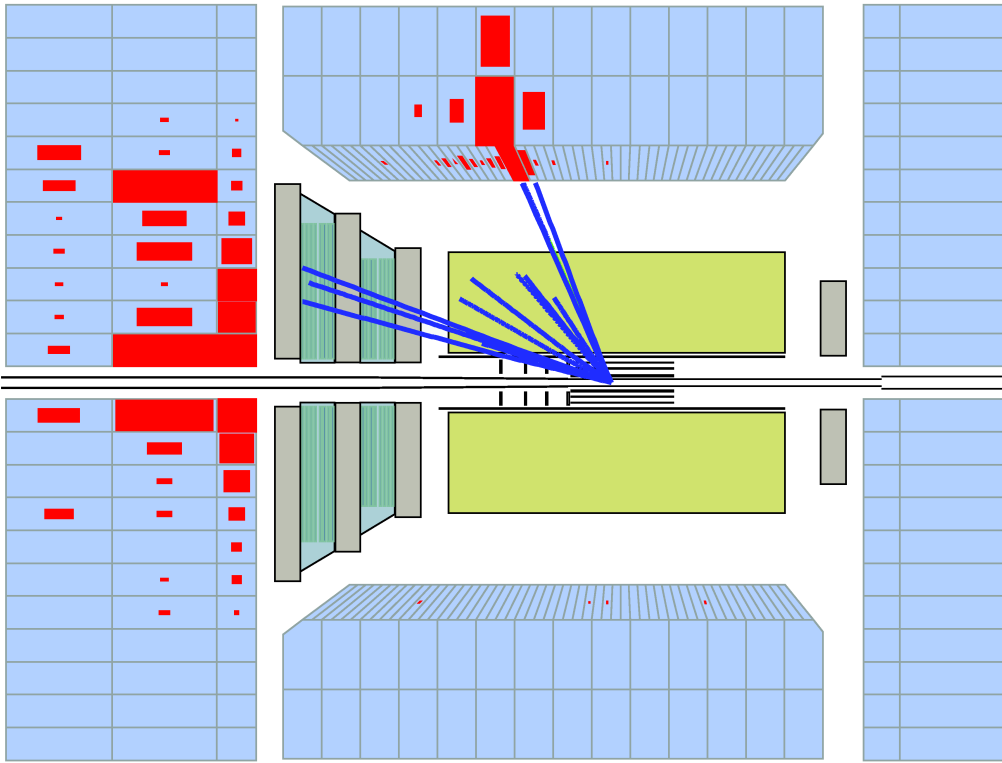


Figure 2: *A charged current event with $Q^2 = 53\,060\text{ GeV}^2$ and $x = 0.59$*

ZEUS

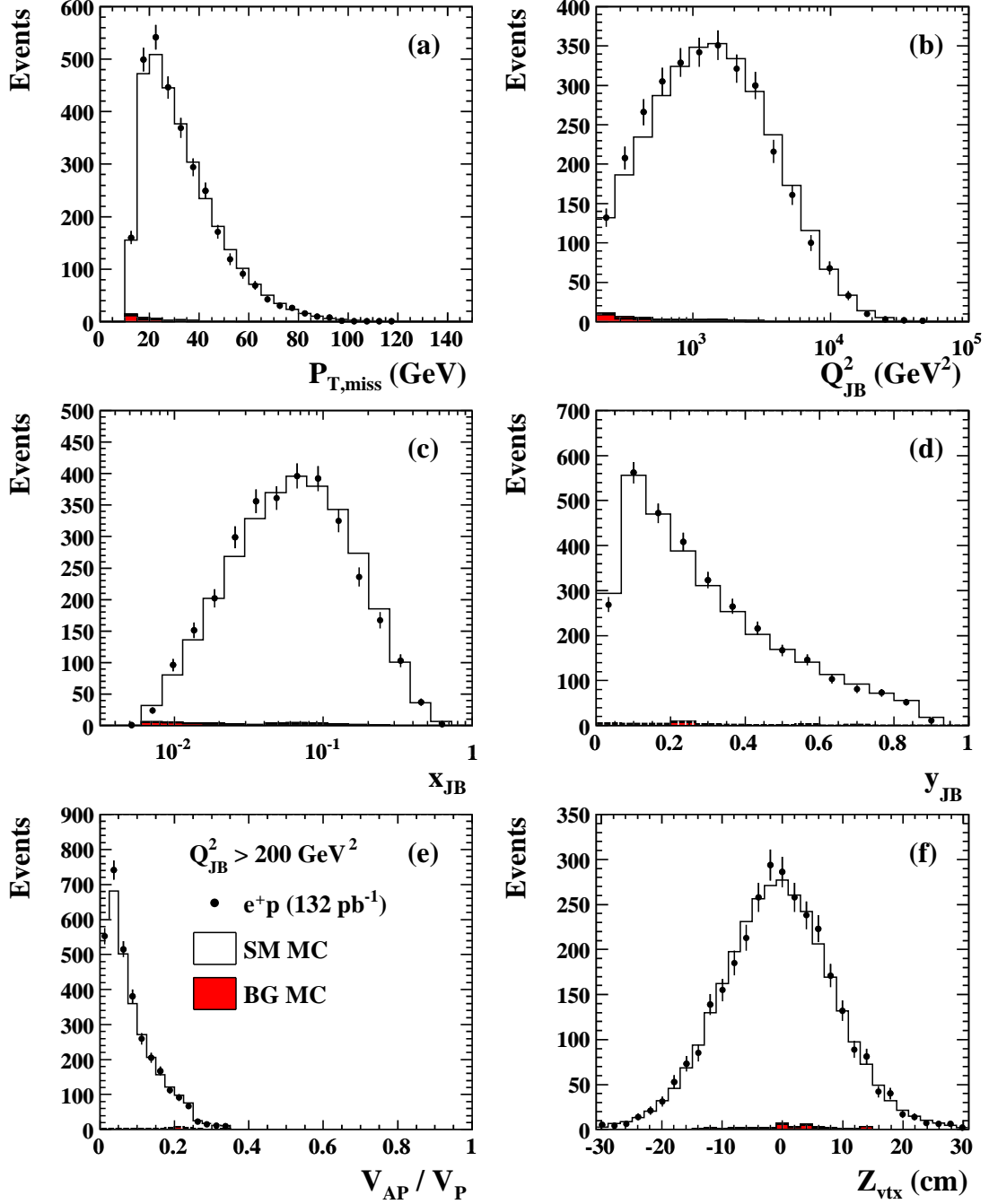


Figure 3: Comparison of the total e^+p CC data sample with the expectations of the Monte Carlo simulation described in the text. The distributions of (a) $P_{T,miss}$, (b) Q_{JB}^2 , (c) x_{JB} , (d) y_{JB} , (e) V_{AP}/V_P and (f) Z_{vtx} , are shown. The points represent data. The open (filled) histograms represent the signal (background) MC.

ZEUS

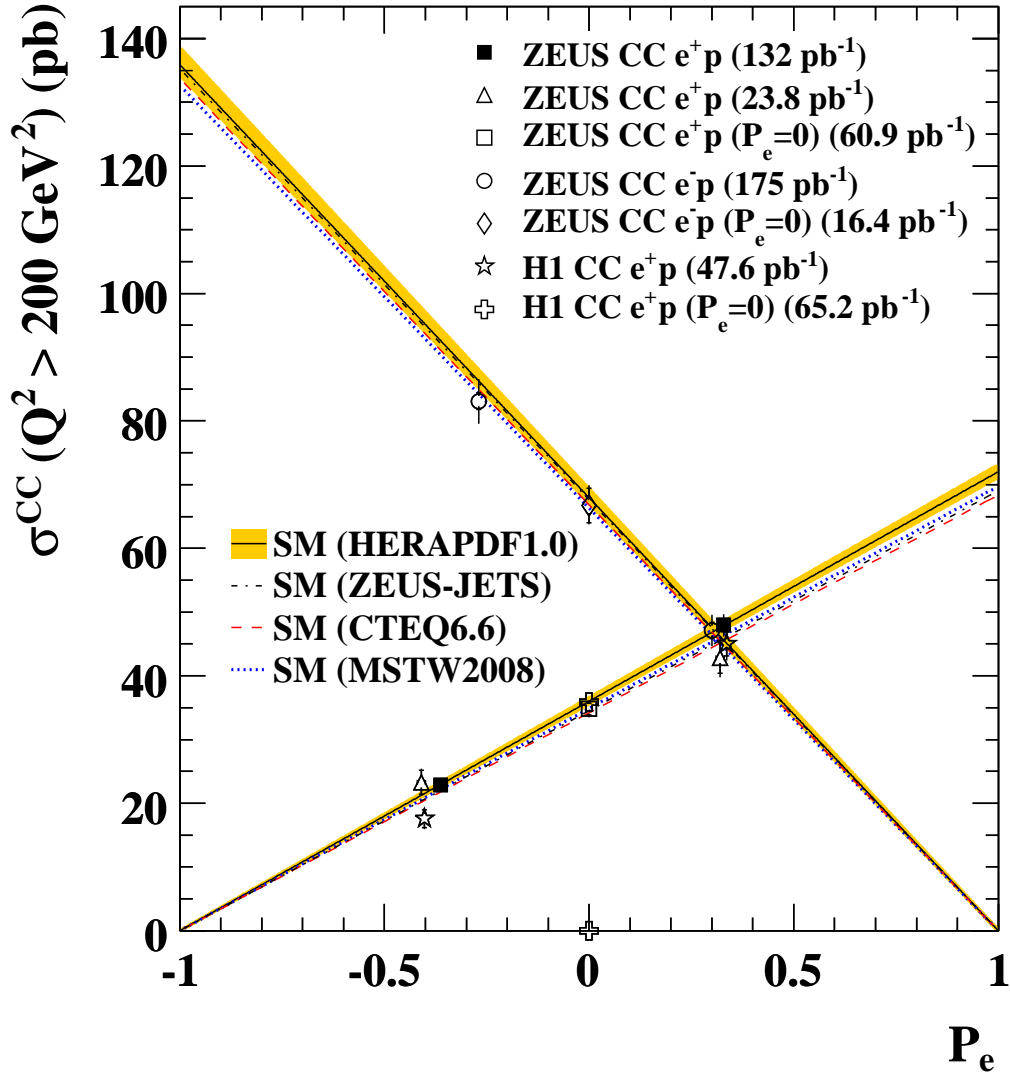


Figure 4: The total cross sections for e^+p (this analysis, filled squares) and e^-p CC DIS as a function of the longitudinal polarisation of the lepton beam. The lines show the SM predictions obtained with HERAPDF1.0, ZEUS-JETS, CTEQ6.6 and MSTW2008 PDFs. The shaded band shows the total uncertainty from the HERAPDF1.0 PDFs.

ZEUS

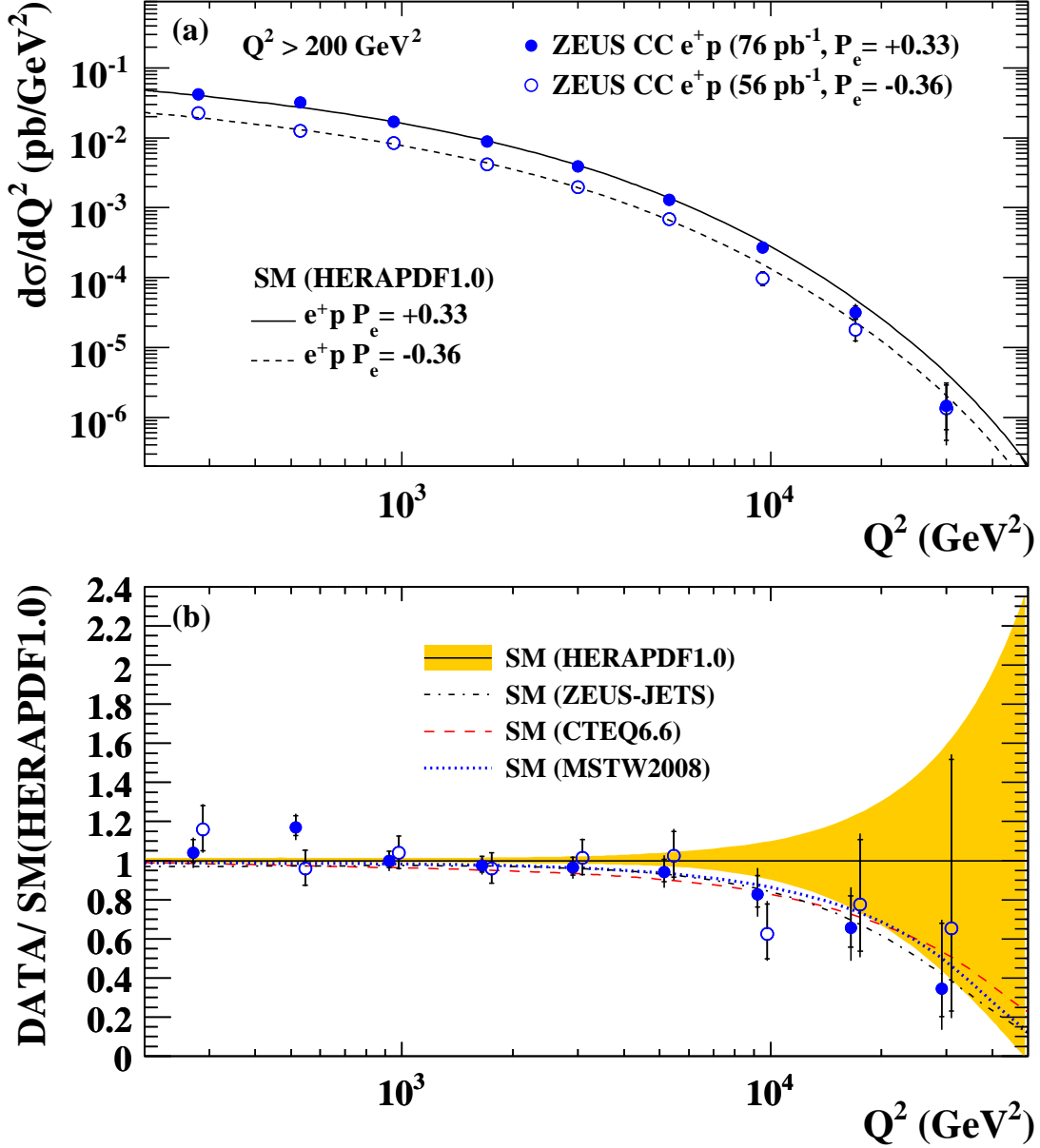


Figure 5: (a) The e^+p CC DIS cross-section $d\sigma/dQ^2$ for data and the Standard Model expectation evaluated using the HERAPDF1.0 PDFs. The positive (negative) polarisation data are shown as the filled (open) points, the statistical uncertainties are indicated by the inner error bars (delimited by horizontal lines) and the full error bars show the total uncertainty obtained by adding the statistical and systematic contributions in quadrature. (b) The ratio of the measured cross-section, $d\sigma/dQ^2$, to the Standard Model expectation evaluated using the HERAPDF1.0 PDFs. The shaded band shows the total uncertainty from the HERAPDF1.0 PDFs. The curves show the ratio of the predictions of the SM evaluated using the ZEUS-JETS, CTEQ6.6 and MSTW2008 PDFs to the prediction from the HERAPDF1.0 PDFs.

ZEUS

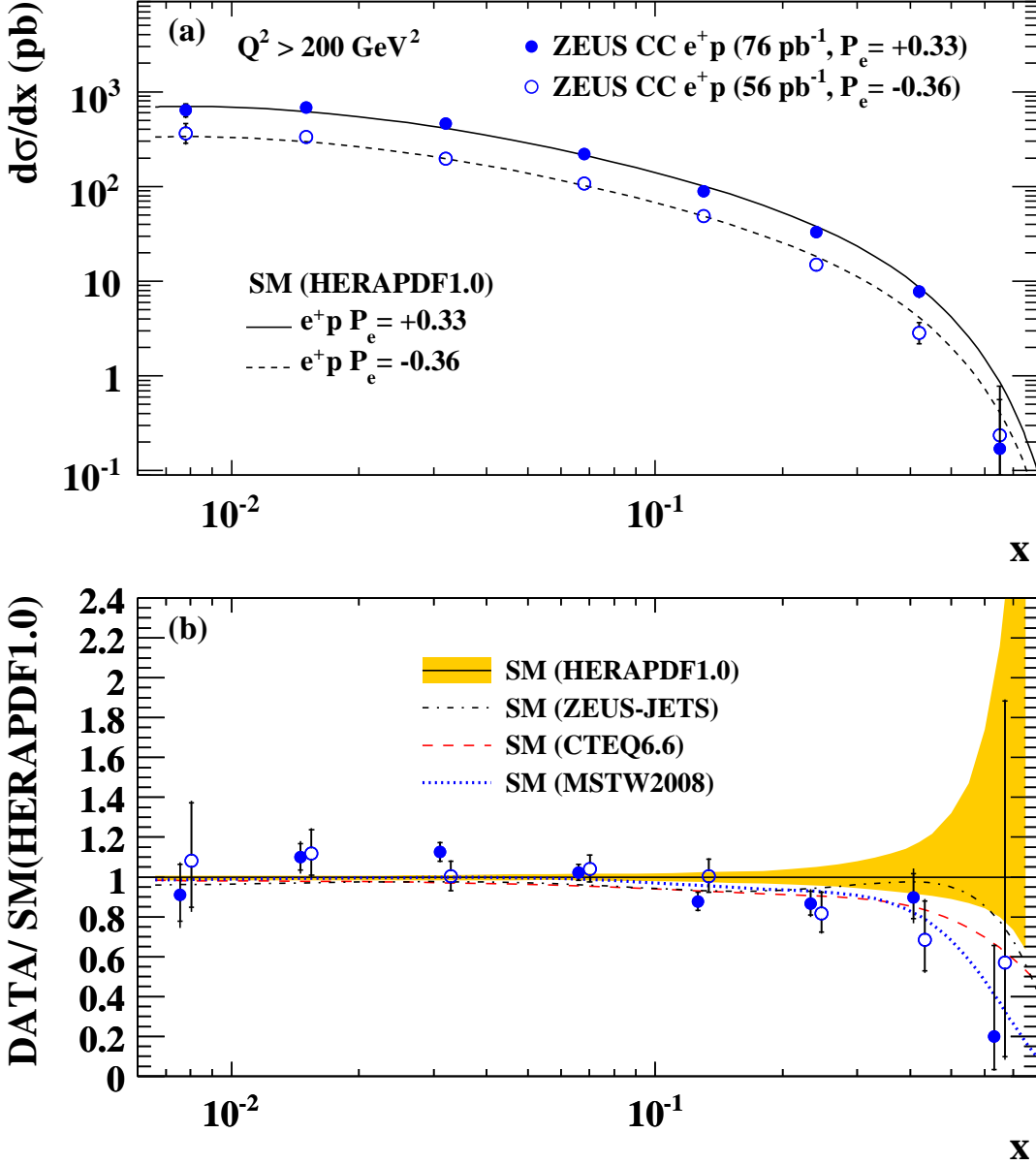


Figure 6: (a) The e^+p CC DIS cross-section $d\sigma/dx$ for data and the Standard Model expectation evaluated using the HERAPDF1.0 PDFs. The positive (negative) polarisation data are shown as the filled (open) points, the statistical uncertainties are indicated by the inner error bars (delimited by horizontal lines) and the full error bars show the total uncertainty obtained by adding the statistical and systematic contributions in quadrature. (b) The ratio of the measured cross-section, $d\sigma/dx$, to the Standard Model expectation evaluated using the HERAPDF1.0 PDFs. The shaded band shows the total uncertainty from the HERAPDF1.0 PDFs. The curves show the ratio of the predictions of the SM evaluated using the ZEUS-JETS, CTEQ6.6 and MSTW2008 PDFs to the prediction from the HERAPDF1.0 PDFs.

ZEUS

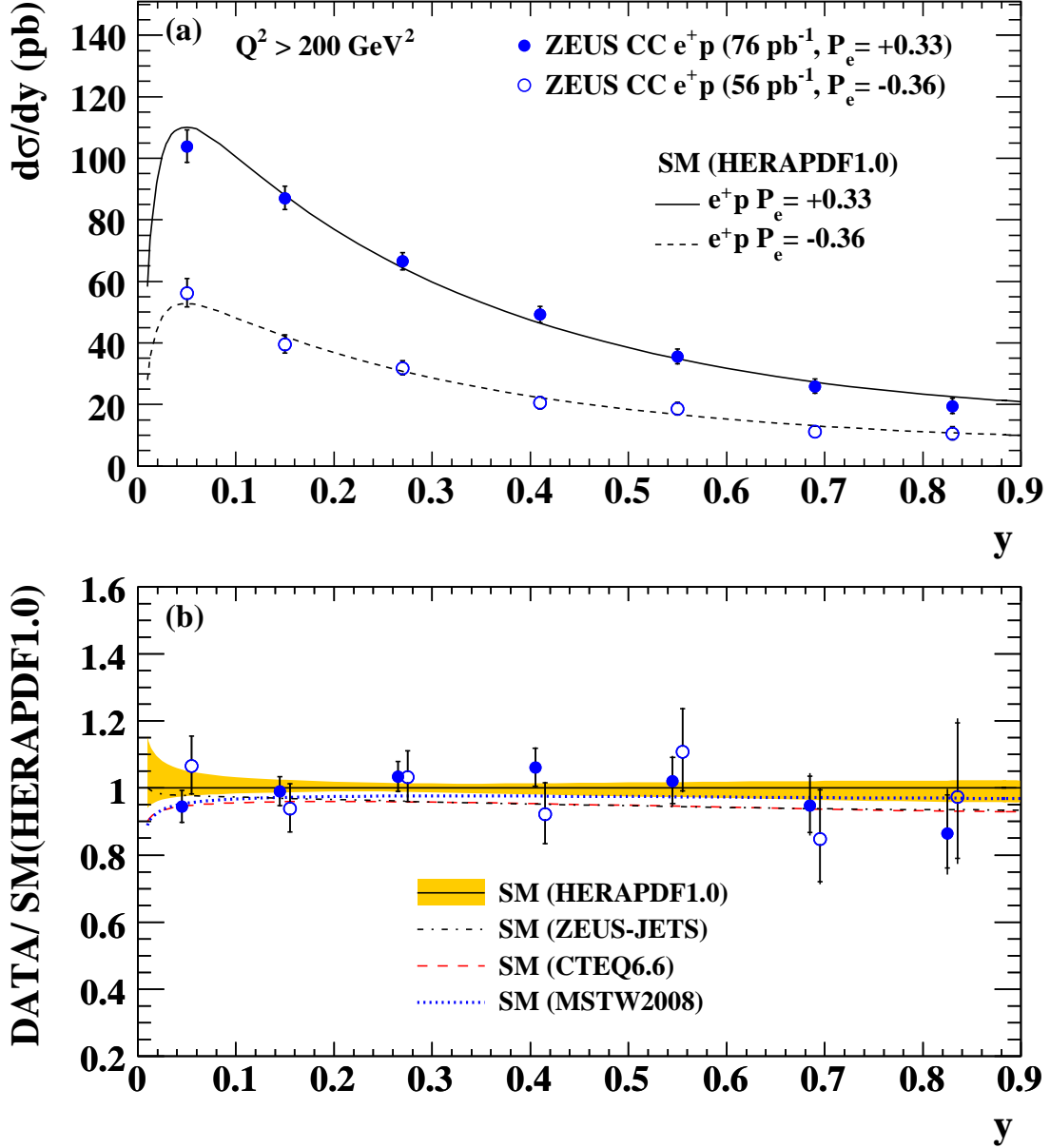


Figure 7: (a) The e^+p CC DIS cross-section $d\sigma/dy$ for data and the Standard Model expectation evaluated using the HERAPDF1.0 PDFs. The positive (negative) polarisation data are shown as the filled (open) points, the statistical uncertainties are indicated by the inner error bars (delimited by horizontal lines) and the full error bars show the total uncertainty obtained by adding the statistical and systematic contributions in quadrature. (b) The ratio of the measured cross-section, $d\sigma/dy$, to the Standard Model expectation evaluated using the HERAPDF1.0 PDFs. The shaded band shows the total uncertainty from the HERAPDF1.0 PDFs. The curves show the ratio of the predictions of the SM evaluated using the ZEUS-JETS, CTEQ6.6 and MSTW2008 PDFs to the prediction from the HERAPDF1.0 PDFs.

ZEUS

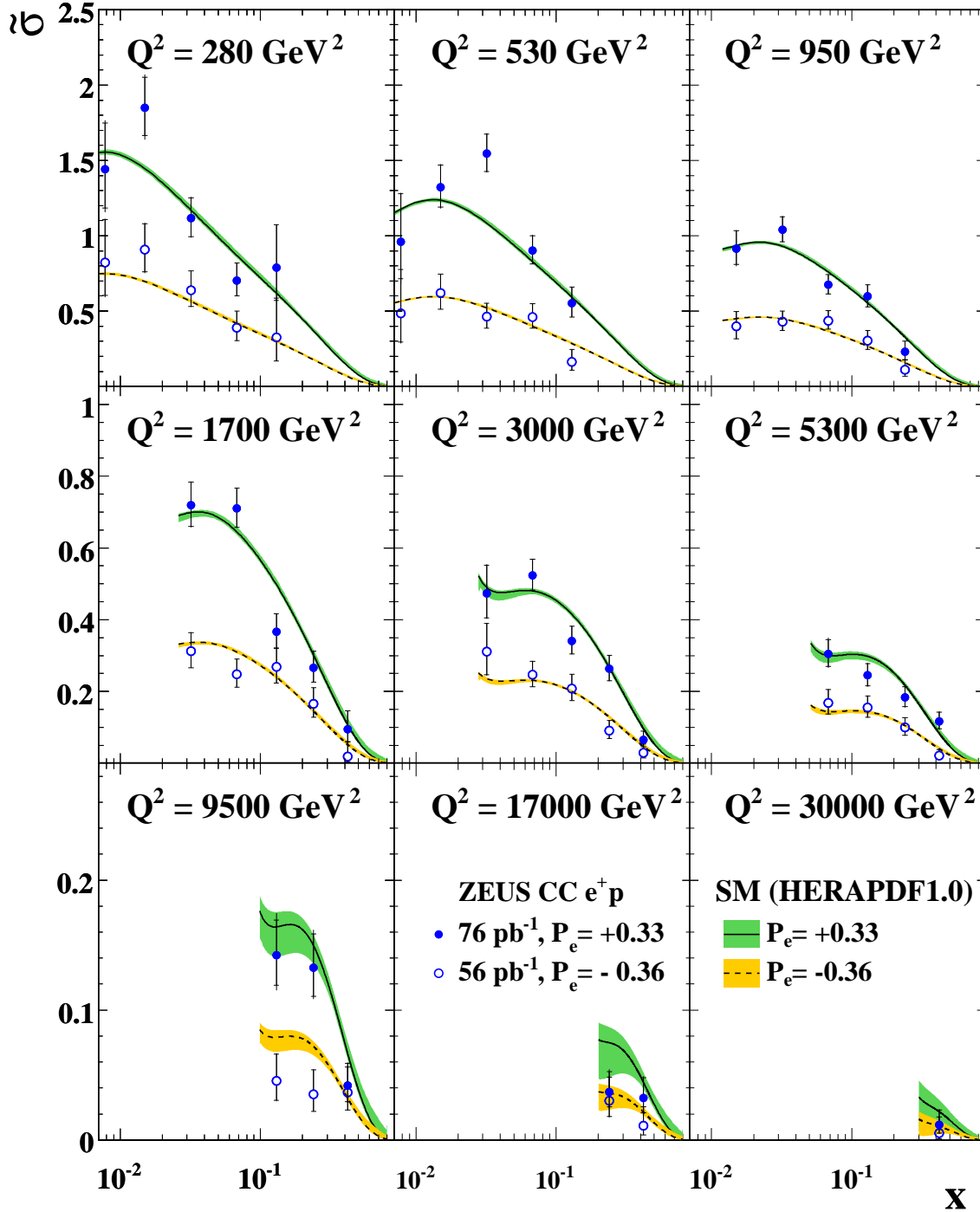


Figure 8: The e^+p CC DIS reduced cross section plotted as a function of x for fixed Q^2 . The positive (negative) polarisation data are shown as the filled (open) points. The curves show the predictions of the SM evaluated using the HERAPDF1.0 PDFs. The shaded bands show the total uncertainty from the HERAPDF1.0 PDFs.

ZEUS

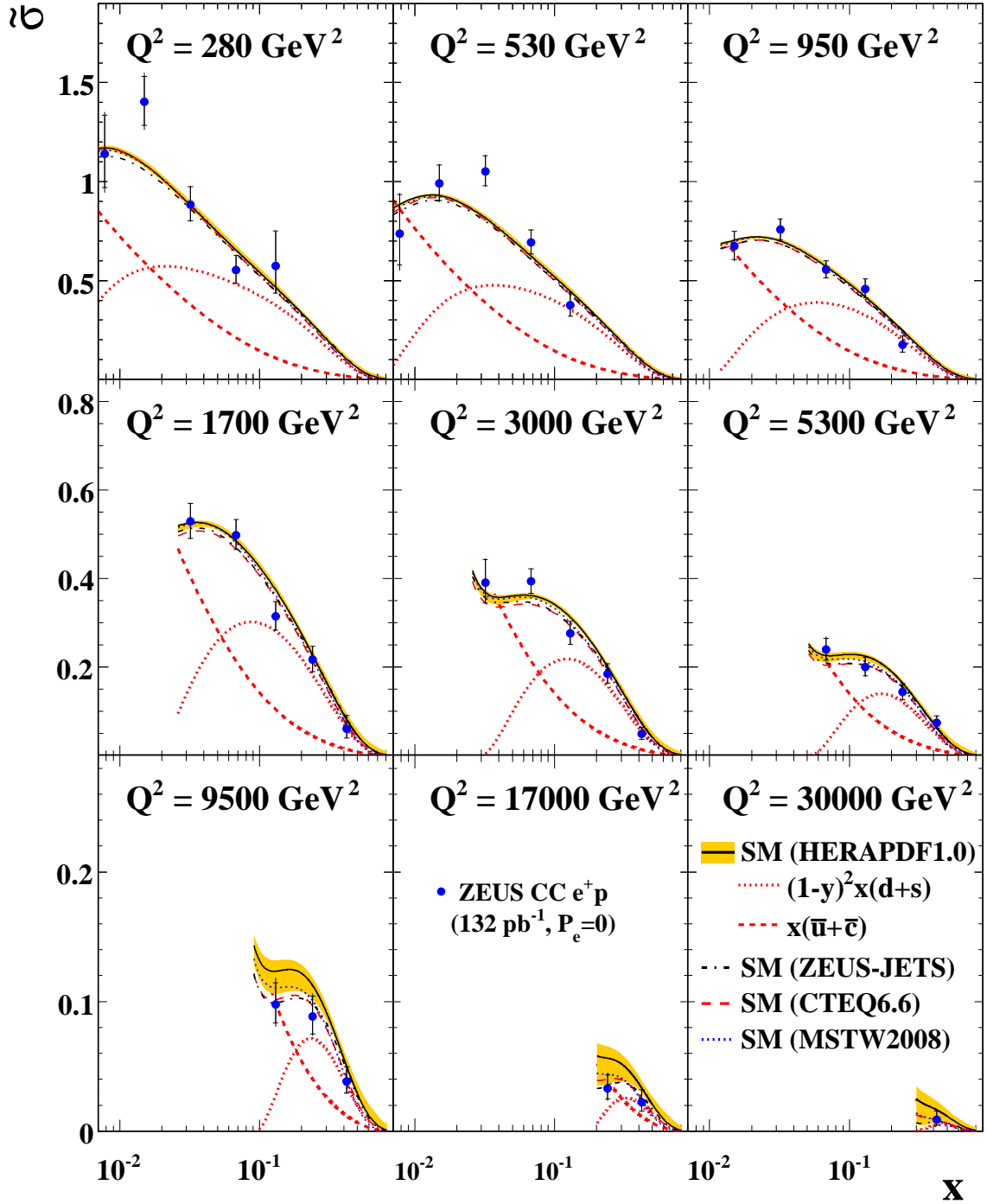


Figure 9: The e^+p CC DIS reduced cross section plotted as a function of x for fixed Q^2 . The circles represent the data points and the curves show the predictions of the SM evaluated using the HERAPDF1.0, ZEUS-JETS, CTEQ6.6 and MSTW2008 PDFs. The dashed and dotted lines show the contributions of the PDF combinations $(1-y)^2 x(d+s)$ and $x(\bar{u} + \bar{c})$, respectively.

ZEUS

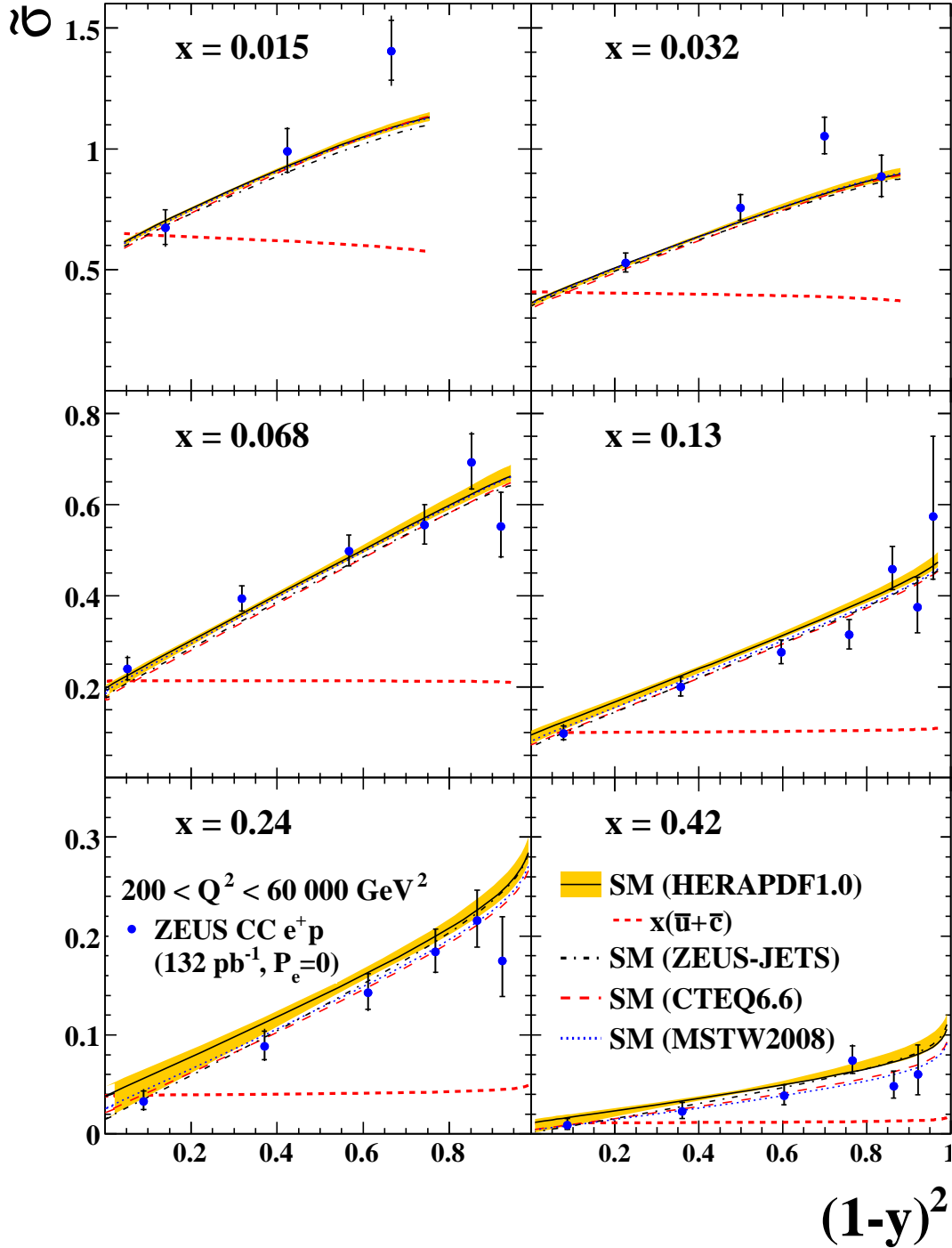


Figure 10: The e^+p CC DIS reduced cross section plotted as a function of $(1-y)^2$ for fixed x . The circles represent the data points and the curves show the predictions of the SM evaluated using the HERAPDF1.0, ZEUS-JETS, CTEQ6.6 and MSTW2008 PDFs. The dashed lines show the contributions of the PDF combination $x(\bar{u} + \bar{c})$ and the shaded band shows the total uncertainty from the HERAPDF1.0 PDFs.

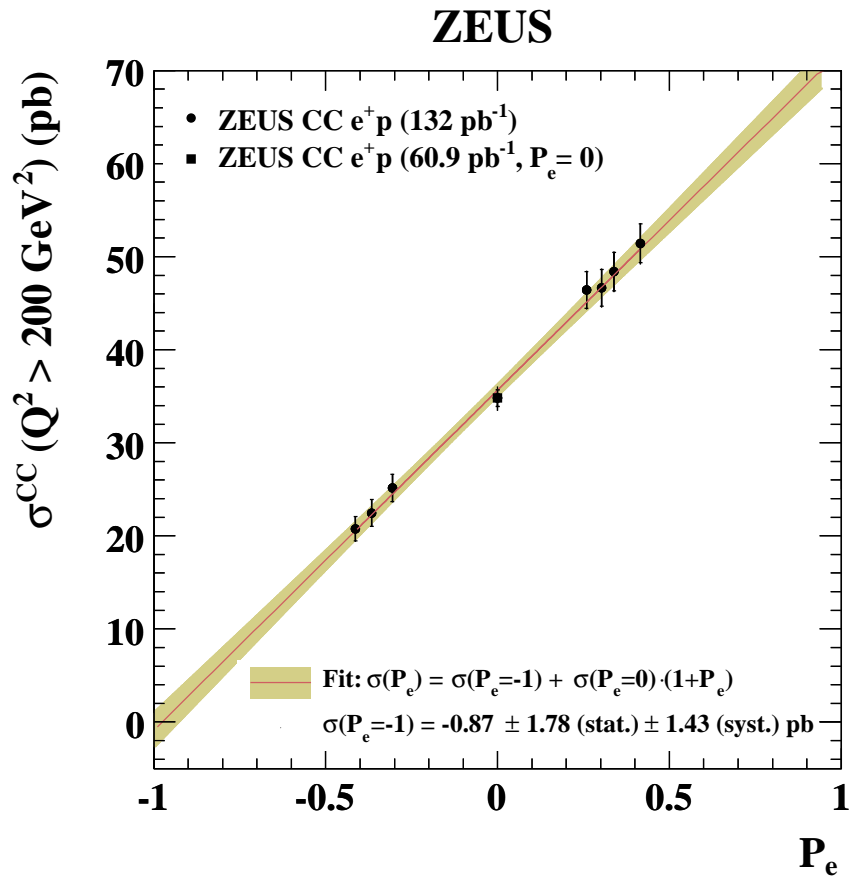


Figure 11: *The total cross sections for e^+p CC DIS as a function of the longitudinal polarisation of the positron beam. The line shows the linear fit to the points and the shaded band shows the uncertainty of the fit.*